

# Design and Synthesis of Curcumin Analogues for in Vivo Fluorescence Imaging and Inhibiting Copper-Induced Cross-Linking of Amyloid Beta Species in Alzheimer's Disease

Xueli Zhang,<sup>†,‡,§</sup> Yanli Tian,<sup>†,||</sup> Zeng Li,<sup>⊥</sup> Xiaoyu Tian,<sup>#</sup> Hongbin Sun,<sup>‡,§</sup> Hong Liu,<sup>⊥</sup> Anna Moore,<sup>\*,†</sup> and Chongzhao Ran<sup>\*,†</sup>

<sup>†</sup>Molecular Imaging Laboratory, MGH/MIT/HMS Athinoula A. Martinos Center for Biomedical Imaging, Department of Radiology, Massachusetts General Hospital/Harvard Medical School, Building 75, Charlestown, Massachusetts 02129, United States

<sup>‡</sup>Center for Drug Discovery, and <sup>§</sup>State Key Laboratory of Natural Medicines, College of Pharmacy, China Pharmaceutical University, Nanjing 210009, China

<sup>||</sup>Department of Parasitology, Zhongshan School of Medicine, Sun Yat-Sen University, Guangzhou, P. R. China

<sup>⊥</sup>State Key Laboratory of Drug Research, Shanghai Institute of Materia Medica, Chinese Academy of Sciences, Shanghai 201203, China

<sup>#</sup>Center for Drug Discovery, Northeastern University, Boston, Massachusetts 02115, United States

## S Supporting Information

**ABSTRACT:** In this article, we first designed and synthesized curcumin-based near-infrared (NIR) fluorescence imaging probes for detecting both soluble and insoluble amyloid beta ( $A\beta$ ) species and then an inhibitor that could attenuate cross-linking of  $A\beta$  induced by copper. According to our previous results and the possible structural stereohindrance compatibility of the  $A\beta$  peptide and the hydrophobic/hydrophilic property of the  $A\beta$ 13–20 (HHQKLVFF) fragment, NIR imaging probe CRANAD-58 was designed and synthesized. As expected CRANAD-58 showed significant fluorescence property changes upon mixing with both soluble and insoluble  $A\beta$  species in vitro. In vivo NIR imaging revealed that CRANAD-58 was capable of differentiating transgenic and wild-type mice as young as 4 months old, the age that lacks apparently visible  $A\beta$  plaques and  $A\beta$  is likely in its soluble forms. According to our limited studies on the interaction mechanism between CRANAD-58 and  $A\beta$ , we also designed CRANAD-17 to attenuate the cross-linking of  $A\beta$ 42 induced by copper. It is well-known that the coordination of copper with imidazoles on Histidine-13 and 14 (H13, H14) of  $A\beta$  peptides could initialize covalent cross-linking of  $A\beta$ . In CRANAD-17, a curcumin scaffold was used as an anchoring moiety to usher the designed compound to the vicinity of H13 and H14 of  $A\beta$ , and imidazole rings were incorporated to compete with H13/H14 for copper binding. The results of SDS-PAGE gel and Western blot indicated that CRANAD-17 was capable of inhibiting  $A\beta$ 42 cross-linking induced by copper. This raises a potential for CRANAD-17 to be considered for AD therapy.



## INTRODUCTION

Alzheimer's disease (AD) has been considered an incurable condition. To date, none of the clinically tested drugs have shown significant effectiveness.<sup>1–4</sup> Therefore, seeking effective therapeutics and imaging probes capable of assisting the drug development are highly desirable.

It is well-known that  $A\beta$  species, including soluble monomers, dimers, oligomers, and insoluble fibrils/aggregates and plaques, play a central role in the neuropathology of AD. Initially, it was thought that insoluble deposits/plaques formed by the  $A\beta$  peptides in AD brain cause neurodegeneration. However, it was later shown that the amyloid plaque burden correlated poorly with AD severity.<sup>5–7</sup> There is recent mounting evidence that soluble dimeric and oligomeric  $A\beta$  species are more neurotoxic than insoluble deposits. Nonethe-

less, both soluble and insoluble  $A\beta$ s are toxic species during the disease progression.<sup>8–10</sup>

Regardless of the nature of the primary contributors to AD pathology, it is widely believed that the initial stage of the full course of amyloidosis is represented by the excessive accumulation of  $A\beta$  monomers caused by imbalanced  $A\beta$  clearance.<sup>11,12</sup> The accumulated monomers gradually aggregate/polymerize/cross-link into neurotoxic soluble dimers and oligomers, the likely biomarkers of the presymptomatic stage, and insoluble fibrils and plaques, the likely biomarkers of the symptomatic stage.<sup>11</sup> In the course of AD progression, all  $A\beta$  species are present, but the predominance of the subspecies

Received: May 24, 2013

Published: October 11, 2013

changes gradually from soluble species to insoluble fibrils and plaques.<sup>8</sup>

Currently, the development of probes for in vivo imaging of insoluble species has been very successful, and a few imaging agents have been approved for clinical use.<sup>2,13–20</sup> However, the availability of imaging probes for the detection of soluble species is still elusive.<sup>21</sup> To fill this gap, we designed and synthesized curcumin analogues CRANAD-58 for detecting not only insoluble  $A\beta$  species but also soluble  $A\beta$  species in vitro and in vivo.

Many molecular imaging probes and drugs share common concepts of design and interaction mechanisms, particularly for probes with the dual function of being a ligand and a fluorophore. For the same target, an imaging probe and a drug could be close analogues.<sup>22</sup> In this report, we also described the design and testing of a CRANAD-58 analogue, which we believe has potential therapeutic effects on AD progression.

High concentrations of metal ions, such as copper and iron, in the brain have been considered as essential factors for the covalent cross-linking of  $A\beta$  and thus an important trigger of the onset of amyloidosis pathology in AD.<sup>23,24</sup> Structurally, two imidazoles of H13 and H14 of an  $A\beta$  peptide serve as essential binding sites for metal coordination.<sup>25–27</sup> This coordination could bring two or more  $A\beta$  peptides into close proximity for initialization of irreversible  $A\beta$  cross-linking.<sup>23,28</sup> Metal ion chelators have been tested for AD treatment with the purpose of retardation of  $A\beta$  aggregation. Clioquinol and its analogue, PBT-2, have been tested in clinical trials.<sup>29,30</sup> Faux et al. reported that PBT-2 could rapidly improve cognition in AD patients.<sup>31</sup> This indicates that metal chelators could hold promise for AD treatment.<sup>32</sup> Other metal chelators with certain specificity toward  $A\beta$  species were also reported as potential inhibitors of  $A\beta$  aggregation.<sup>33–36</sup>

However, one of the obvious and potential side effects of the metal chelators is the disruption of brain metal homeostasis during a prolonged treatment.<sup>30,37</sup> Structurally, all of the reported chelators are bi- or tridentate ligands for metal ions; therefore a single molecule could coordinate with a metal ion to form an intramolecular complex. Before reaching the target (or targeting region), they could sequester/seize metal ions that may be essential for normal brain functions. In this report we used a different approach, which was based on our limited investigation of the interaction mechanism of the designed imaging probe with  $A\beta$  and its fragments. Here we designed and synthesized a curcumin analogue termed CRANAD-17, in which a curcumin scaffold was used as an anchoring moiety to usher the designed compound to the vicinity of H13 and H14 of  $A\beta$ , and imidazole rings were incorporated to compete with H13/H14 within  $A\beta$  for copper binding. Unlike the traditional chelators, CRANAD-17 is monodentate, and a single molecule could not chelate/seize a metal ion to form an intramolecular metal complex. Therefore, we expect that the disruption of brain metal homeostasis/balance by CRANAD-17 would be minimal.

## RESULTS

**Design and Synthesis of Imaging Probes.** To design a soluble  $A\beta$  species sensitive imaging probe, we first explored the structural stereohindrance compatibility of  $A\beta$  species. In our previous studies, we designed a curcumin-based near-infrared (NIR) fluorescence imaging probe, CRANAD-2, and showed that this probe was able to differentiate 19 month old wild-type and transgenic mice using in vivo NIR imaging.<sup>38</sup>

CRANAD-2 could be considered a “smart” probe because it displayed a significant fluorescence intensity increase, an emission blue shift, a lifetime change, and quantum yield improvement upon interacting with insoluble  $A\beta$  aggregates.<sup>38</sup> However, we found that CRANAD-2 lacks the capability of detecting soluble  $A\beta$  species. After incubation of soluble  $A\beta$  species (monomeric  $A\beta$ 40 were used as representative species, SI Figure 1) with CRANAD-2, no significant fluorescence property change was detected (Figure 1a, red line). Of note,

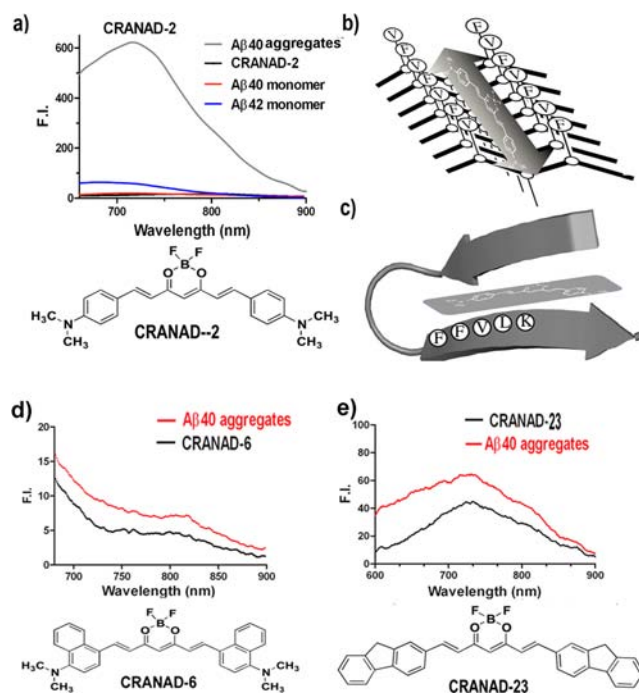


**Figure 1.** Fluorescence spectra of (a) CRANAD-2 alone (black, overlapped with red line), with  $A\beta$ 40 aggregates (gray) and with  $A\beta$ 40 monomers (red), and  $A\beta$ 42 monomers (blue) (of note, no significant fluorescence changes were observed with the monomers). (b–c) Two proposed binding sites (site A and B) for CRANAD-2 inside  $A\beta$ 40 aggregates. (b) Hydrophobic channel (site A) formed by hydrophobic amino acid residues such as F (phenylalanine) and V (valine). (c) Hydrophobic core fragment (KLVFF) (site B) inside  $A\beta$ 40/42 peptide. CRANAD-2 could possibly be intercalated between the  $\beta$ -sheets. (d) Fluorescence spectra of CRANAD-6 alone (black) and with  $A\beta$ 40 aggregates (red). (e) Fluorescence spectra of CRANAD-23 alone (black) and with  $A\beta$ 40 aggregates (red). Of note, there were no significant fluorescence changes in CRANAD-6, and -23 interactions with  $A\beta$ 40 aggregates.

CRANAD-2 exhibited an emission blue shift upon interacting with  $A\beta$  aggregates/fibrils (Figure 1a, gray line), indicating that it binds to a hydrophobic microenvironment.<sup>39,40</sup> Inside  $A\beta$  fibrils, we suggest the existence of two possible major hydrophobic sites (site A and B) (Figure 1b,c). Site A is comprised of multiple hydrophobic residues (such as phenylalanine) along the long axis of the fibrils (Figure 1b).<sup>41</sup> Site B contains the core fragment (KLVFF) of an  $A\beta$ 40/42 peptide (Figure 1c). Structurally, site A is more stereohindrance compatible than site B. Presumably, by extending the aromatic ring of CRANAD-2 when it binds to site A (Figure 1b), it would retain its binding to the hydrophobic site and consequentially retain its fluorescence response to  $A\beta$  aggregates/fibrils.

To investigate this assumption, we synthesized compounds CRANAD-6 and -23, which are analogues of CRANAD-2 with extended aromatic rings. No significant fluorescence changes were observed upon incubation of these two compounds with  $A\beta$  aggregates/fibrils in solution (Figure 1d,e), suggesting that: (1) CRANAD-2 and its analogues probably are not binding to the hindrance compatible site A (Figure 1b); (2) the binding site of CRANAD-2 inside the  $A\beta$  fibrils is stereohindrance sensitive, because analogues like CRANAD-6 and -23 with bulky aromatic ring moieties are not able to access the binding site; and (3) the fluorescence response of CRANAD-2 to  $A\beta$  aggregates/fibrils probably originates from the interaction of the probe with site B, which is structurally hindrance sensitive to the ligand (Figure 1c). Given that CRANAD-2 showed a significant fluorescence responses to  $A\beta$  aggregates/fibrils but not to monomeric  $A\beta$ , we concluded that the interaction between site B of monomeric  $A\beta$ 40 and CRANAD-2 was most likely weak. We reasoned that this weak interaction could be due to the structure of CRANAD-2 that did not match the hydrophobic and hydrophilic properties of site B, which may span from H13 to F20 (i.e.,  $A\beta$ 13–20) and include the hydrophilic segment HHQK and hydrophobic segment LVFF. We also reasoned that half of the CRANAD-2 molecule (CRANAD-54) should have a strong interaction with the hydrophobic LVFF segment and have stronger fluorescence responses upon interaction with monomeric  $A\beta$  (Figure 2a).

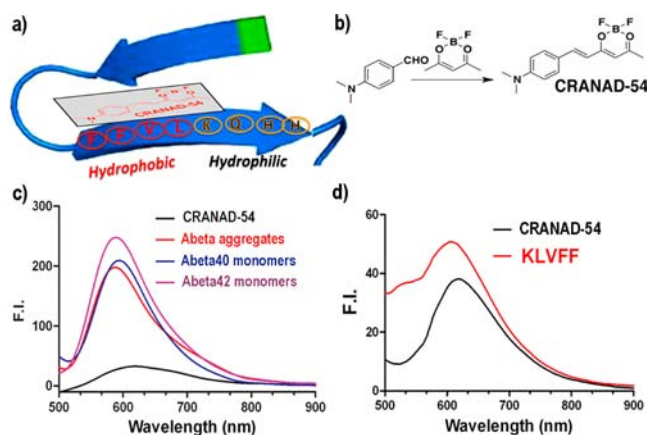


**Figure 2.** (a) The proposed interaction model between CRANAD-54 and  $A\beta$ . (b) Synthetic route of CRANAD-54. (c) Fluorescence spectra of CRANAD-54 alone (black) and with  $A\beta$ 40 monomers (purple),  $A\beta$ 42 monomers (blue) and  $A\beta$ 40 aggregates (red). (d) Fluorescence spectra of CRANAD-54 alone (black) and with  $A\beta$ 16–20 (KLVFF) fragment (red).

To verify our hypothesis, CRANAD-54 was synthesized (Figure 2b) and tested with monomeric  $A\beta$ 40/42 (Figure 2c) and the hydrophobic core fragment KLVFF (Figure 2d). As expected, CRANAD-54 showed significant fluorescence changes with KLVFF and much stronger fluorescence intensity increase with monomeric  $A\beta$ 40 than CRANAD-2 (Figure 2c). To test the specificity of CRANAD-54 toward the KLVFF fragment, we tested the control  $A\beta$  fragment ( $A\beta$ 22–35) and observed no significant response (SI Figure 2), indicating CRANAD-54's specificity toward the core fragment. Nonetheless, CRANAD-54 was not suitable for in vivo imaging due to its short excitation and emission wavelengths. To further develop a probe that would be responsive to soluble  $A\beta$  species and suitable for in vivo NIR imaging, a longer  $\pi$  conjugation system

is needed for pushing excitation and emission into NIR region, while the extended conjugation part should match the hydrophilic property of the HHQK segment. To this end, we designed an asymmetric curcumin analogue, CRANAD-58, in which the CRANAD-54 moiety was used to interact with the hydrophobic LVFF, and the hydrophilic pyridyl moiety was conjugated to match the hydrophilic HHQK segment and to extend the  $\pi$  conjugation (Figure 3a). In addition, we assumed

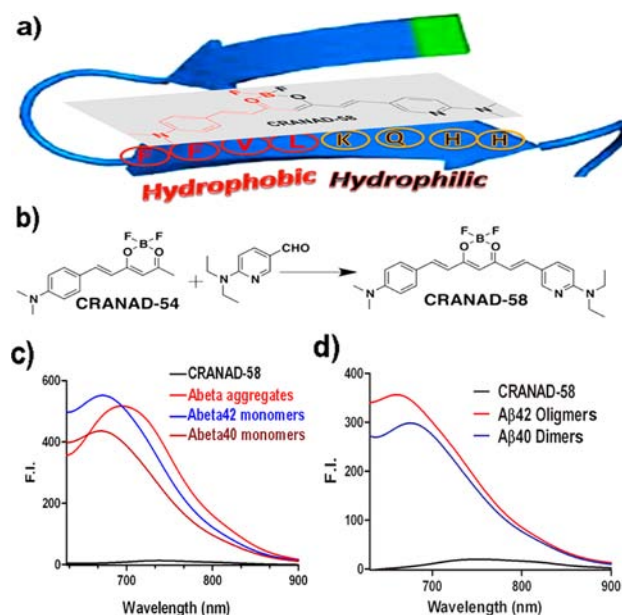


**Figure 3.** (a) The proposed interaction model between CRANAD-58 and  $A\beta$ . (b) Synthetic route of CRANAD-58. (c) Fluorescence spectra of CRANAD-58 alone (black) and with  $A\beta$ 40 monomers (deep red),  $A\beta$ 42 monomers (blue), and  $A\beta$ 40 aggregates (red). (d) Fluorescence spectra of CRANAD-58 alone (black) and with  $A\beta$ 40 dimers (blue) and  $A\beta$ 42 oligomers (red).

that the nitrogen of the pyridyl ring could form a hydrogen bond with the HHQK fragment and thus enhance the binding.<sup>42,43</sup> CRANAD-58 was synthesized by conjugating CRANAD-54 with 6-( $N,N'$ -diethylamino)-3-formyl-pyridine (Figure 3b), and its structure was confirmed by  $^1\text{H}$ ,  $^{13}\text{C}$ , and  $^{19}\text{F}$  NMR and MS spectra.

**In Vitro Characterization of CRANAD-58.** CRANAD-58 displayed an excitation peak at  $\sim 630$  nm and an emission peak at  $\sim 750$  nm (SI Figure 3), which are suitable for in vivo NIR imaging. As expected, CRANAD-58 showed an excellent fluorescence response toward soluble species such as  $A\beta$  monomers (Figure 3c). It displayed a 91.9- and 113.6-fold fluorescence intensity increase at 672 nm for  $A\beta$ 40 and  $A\beta$ 42 monomers, respectively. CRANAD-58 also showed a significant emission wavelength shift upon mixing with these soluble species. Moreover, we also found that CRANAD-58 exhibited strong binding with  $A\beta$  monomers ( $A\beta$ 40:  $K_d = 105.8$  nM,  $A\beta$ 42:  $K_d = 45.8$  nM).

Shankar et al. has recently showed that  $A\beta$  dimers extracted from AD patients are highly toxic species for neurons. These dimers potently inhibited long-term potentiation (LTP), enhanced long-term depression and reduced dendritic spine density in normal rodent hippocampus.<sup>10</sup> Since CRANAD-58 showed significant fluorescence property changes with monomeric  $A\beta$ s, it was important to test whether the probe had similar responses toward dimers. To this end, we used



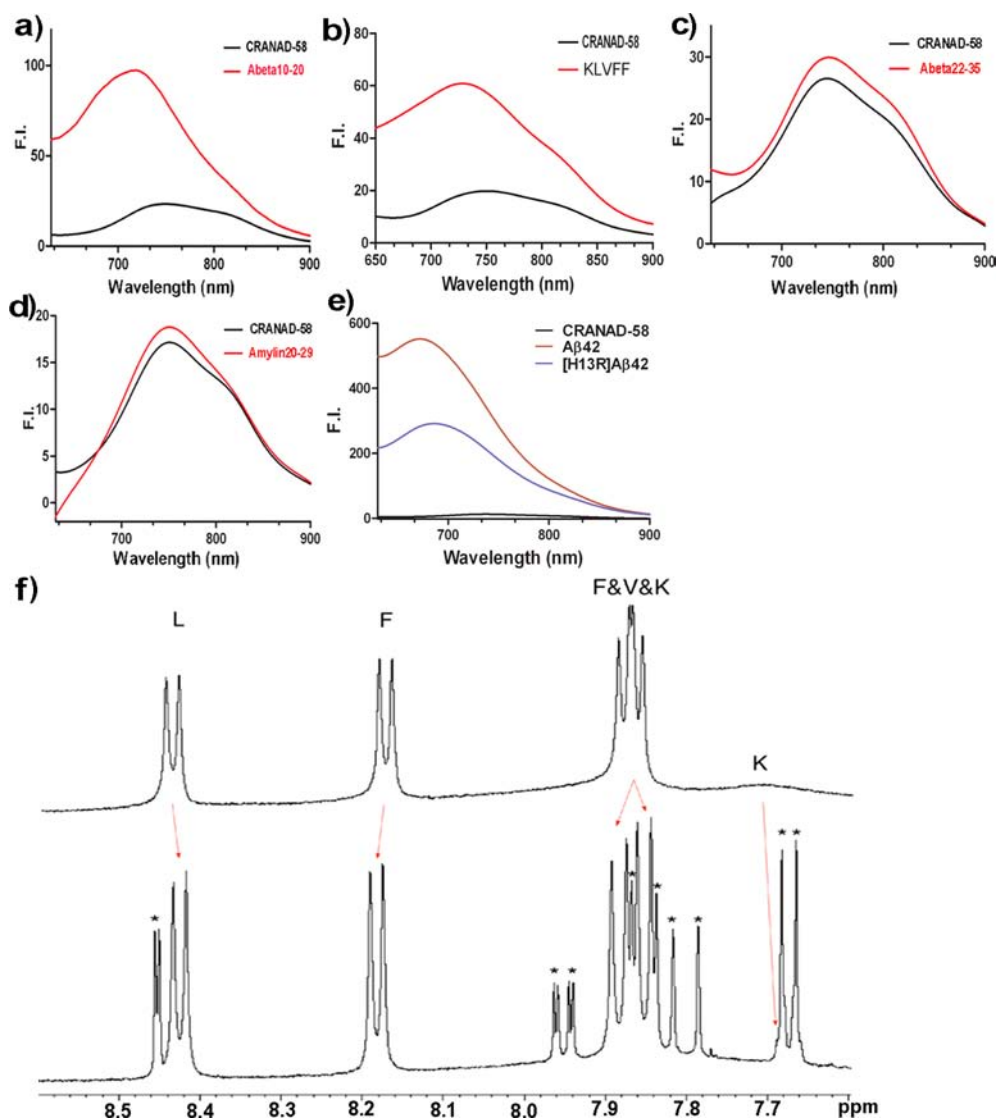


**Figure 4.** (a–e) Fluorescence spectra of CRANAD-58 with Aβ10–20 (a), Aβ16–20(b), Aβ22–35 (c), Amylin 20–29 (d), and [H13R]Aβ42 (e). (f) <sup>1</sup>H NMR spectra of Aβ16–20 only (top) and with CRANAD-58 (bottom). \* Indicated that the peaks originated from ligand CRANAD-58.

synthetic dimers of Aβ<sub>40</sub>-S26C (in which serine 26 was mutated to cysteine). Shankar et al. showed that this soluble dimer could significantly inhibit LTP, indicating its strong neurotoxicity. We found that CRANAD-58 had a significant fluorescence intensity increase (~60-fold) and emission blue-shifts upon mixing with the dimers (Figure 3d, blue line). However, compared to the intensity of CRANAD-58 with Aβ<sub>40</sub> or Aβ<sub>42</sub> monomer, it displayed lower intensity with S26C-Aβ<sub>40</sub> dimers (Figure 3c,d), indicating that the cross-linking at the S26C position partially disturbed the probe binding.

In recent years, mounting evidence indicates that soluble oligomers are highly toxic for neurons.<sup>8–10</sup> Therefore, the next step in our investigation was to test whether CRANAD-58 could interact with soluble Aβ oligomers. We prepared Aβ<sub>42</sub> oligomers according to the procedure reported by Kaye<sup>44</sup> and confirmed the morphology of obtained species by transmission electron microscopy (TEM) (SI Figure 1d). Similar to other soluble Aβs, CRANAD-58 showed an apparent fluorescence intensity increase and emission peak shift (Figure 3d, red line). However, the intensity was lower than that with monomeric Aβs, probably due to the fact that CRANAD-58 could have

lower responses for oligomers with certain secondary structures.

In addition, CRANAD-58 displayed a significant intensity increase and wavelength shift upon interaction with insoluble Aβ<sub>40</sub> aggregates (Figure 3c). Interestingly, the emission peaks from monomeric and aggregated Aβs were apparently different. To test whether the emission peaks could shift with different relative content of monomeric and aggregated Aβs, 100%, 70%, 50%, 30%, and 0% aggregates were prepared for titration. As expected, the emission peaks of CRANAD-58 shifted toward shorter wavelengths with the decreased amount of aggregates. These data indicated that CRANAD-58 could detect coexisting soluble and insoluble Aβs (SI Figure 4a).

To investigate the specificity of CRANAD-58 for Aβ species, amylin (an aggregation-prone 37-residue peptide secreted by pancreatic β-cells together with insulin)<sup>45</sup> was used as a control peptide. A significantly lower fluorescence intensity increase was observed when CRANAD-58 was incubated with this peptide, suggesting its excellent selectivity toward Aβ species (SI Figure 4b).

**Limited Interaction Mechanism Studies with CRANAD-58.** To further investigate the interaction mechanism, we made an effort to identify the segment within the peptide that was essential for the binding. Based on our design hypothesis, CRANAD-58 should have interaction with A $\beta$ 13–20. To verify this assumption, we used commercially available A $\beta$ 10–20 as an alternative for testing. Indeed, it displayed strong fluorescence intensity increase upon mixing with A $\beta$ 10–20 (Figure 4a). Segment A $\beta$ 16–20 (KLVFF) has the highest hydrophobicity within the peptide and is widely considered as the core segment for the aggregation process.<sup>46</sup> We also tested the probe with this segment. To exclude any possible response from its aggregated form, the nonaggregating morphology of A $\beta$ 16–20 was confirmed by TEM (SI Figure 1). Upon incubation with this segment, CRANAD-58 displayed a significant fluorescence intensity increase (~3-fold) and an apparent emission blue-shift, indicating that the probe had specific interaction with the KLVFF segment (Figure 4b).

To further confirm that the fluorescence property changes originated from the KLVFF segment, we tested CRANAD-58 with a non-KLVFF containing peptide A $\beta$ 22–35.<sup>46</sup> No significant change in fluorescence intensity was observed with this peptide (Figure 4c). Based on the above results, we concluded that the KLVFF fragment was most likely the core structure for the observed interaction. In addition, we also tested CRANAD-58 with the core fragment of Amylin (Amylin 20–29),<sup>46</sup> an aggregating-prone 37-amino acid peptide, and observed no significant fluorescence property change (Figure 4d).

The interaction between CRANAD-58 and the KLVFF fragment was further confirmed by NMR spectroscopy, which demonstrated significant shift in signals from amide protons of K, V, and F<sup>43,47</sup> (Figure 4f). The NMR data again suggested that CRANAD-58 specifically interacts with the core fragment.

Once we obtained the evidence for the interaction between CRANAD-58 and the KLVFF fragment, we tested whether it could interact with the hydrophilic HHQK moiety. To this end, we compared the fluorescence intensities of CRANAD-58 with A $\beta$  and H13R substituted A $\beta$  ([H13R]A $\beta$ ), in which H13 was replaced by arginine (R). As expected, a significantly lower fluorescence intensity was observed for [H13R]A $\beta$ , suggesting that CRANAD-58 specifically interacted with H13 (Figure 4e).

Based on fluorescence and NMR studies, we proposed an interaction model shown in SI Figure 5a, in which K16 and L17 interact with the boron-diketone motif, and VFF moiety forms a hydrophobic interaction with the phenyl ring of CRANAD-58. To investigate whether the proposed model was reasonable, we conducted docking experiments for CRANAD-58 and A $\beta$ . The contact model between CRANAD-58 and A $\beta$  is shown in SI Figure 5b,c. As suggested from the experimental data, half of the CRANAD-58 molecule formed hydrophobic interactions with the hydrophobic LVFF segment. Two hydrogen bonds were formed between CRANAD-58 with K-16 and L-17, separately. The pyridyl moiety and the corresponding substituents from the other half of the molecule interacted with the HHQK hydrophilic segment. Moreover, another hydrogen bond was formed between the nitrogen on the pyridyl ring with Q-15 of main chain. This pattern demonstrated that the whole molecule interacted with the  $\beta$ -sheet segment by both electrostatic and hydrophobic contacts, while the introduction of the pyridyl ring enhanced the binding affinity. Although the docking result indicated that the pyridyl moiety interacted with H14, the expected interaction with H13

was not observed. The docking result was partially consistent with the experimental data.

**Histological Studies with CRANAD-58.** To test whether CRANAD-58 could specifically interact with A $\beta$  species in a biologically relevant environment, we stained a brain slice from an 18 month old APP/PS1 transgenic mouse. As shown in microscopic images in Figure 5, CRANAD-58 could specifically highlight A $\beta$  plaques demonstrating excellent colocalization with Thioflavin S staining, the gold standard staining for A $\beta$  plaques.

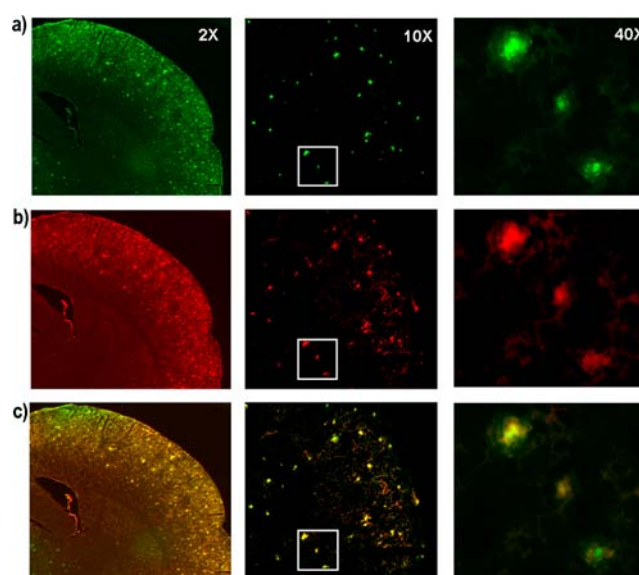


**Figure 5.** Histological staining of the brain slices from an 18 month old APP/PS1 transgenic mouse. (a) Staining with Thioflavin T indicated abundant plaques in the cortex region. Magnification: left –2 $\times$ , middle –10 $\times$ , right –40 $\times$  showing the region outlined in 10 $\times$  image. (b) Staining with CRANAD-58; (c) Merged images of b and c.

**In Vivo Imaging with CRANAD-58 in 4 Month Old APP/PS1 Mice.** As a brain imaging probe, CRANAD-58 must meet several necessary requirements that include proper lipophilicity (log *P*) and reasonable BBB penetration.<sup>38</sup> We found that log *P* = 1.94 for CRANAD-58, which was reasonable for brain imaging. To investigate whether CRANAD-58 was capable of penetrating BBB, we acquired LC-MS and fluorescence spectra from the brain homogenate extraction obtained from mice intravenously injected the probe and perfused with PBS. The LC retention times and MS spectra of the extraction were the same as with the standard CRANAD-58. The fluorescence spectra of the extraction and standard CRANAD-58 spectra were similar as well, suggesting that CRANAD-58 was able to penetrate the BBB (SI Figure 6).

To investigate whether CRANAD-58 had the capacity to detect A $\beta$  species in mouse brain, we first conducted phantom imaging with wild-type mouse brain. In this experiment, a dissected wet brain was divided into two even halves and homogenized, and then synthetic A $\beta$  monomers or oligomers were added to the homogenate. We found that the signal of CRANAD-58 was about 1.3-fold higher with A $\beta$ s than without A $\beta$ s (SI Figure 7a), suggesting that the probe could be used for further in vivo testing with transgenic mice.

APP/PS1 mice, the most studied transgenic AD mouse model,<sup>48–50</sup> were used to test the utility of CRANAD-58 for in vivo NIR imaging. This mouse model possesses double

humanized APP/PS1 genes and constantly produces considerable amounts of “human”  $A\beta$  species. Previous studies indicated that APP/PS1 mice have no significant  $A\beta$  deposits/plaques before 6 months of age. It is believed that the majority of  $A\beta$  species in mice younger than 6 months are soluble.<sup>49</sup> To test whether CRANAD-58 was able to detect soluble species in vivo by NIR imaging, we used 4 month old APP/PS1 mice. After intravenous injection, we found that fluorescence signals from the brains of APP/PS1 mice were significantly higher than that from the age-matched wild-type mice at all time points used (Figure 6a). The signals from APP/PS1 mice (Figure 6a)

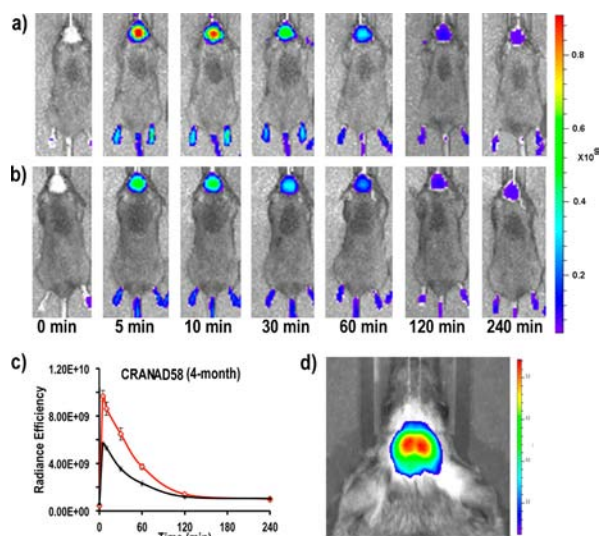


**Figure 6.** Representative images of APP-PS1 transgenic and wild-type control mice at different time points before and after i.v. injection with 2.0 mg/kg of CRANAD-58 (images of all mice showed in SI Figure 7b). (a) 4 month old APP-PS1 mouse. (b) 4 month old control mouse. (c) Quantitative analysis of fluorescence signals from transgenic APP/PS1 and control mice ( $n = 3-4$ ) at preinjection and 5, 10, 30, 60, 120, and 240 min after i.v. injection. The signals were significantly higher in 4 month old APP/PS1 mice than that in the age-matched control mice. (d) Representative high-resolution image of an APP/PS1 mouse injected with CRANAD-58.

were 1.71-, 1.62-, 1.82-, 1.60-, and 1.17-fold of the signals from wild-type controls at 5, 10, 30, 60, and 120 min after injection (Figure 6b, and SI Figure 7b), suggesting that CRANAD-58 indeed was capable of detecting soluble  $A\beta$  species in vivo.

To further validate the in vivo imaging results, we conducted an ELISA test to determine the  $A\beta$  content in brain homogenate from the imaged mice. The difference in total  $A\beta$  content between APP/PS1 and wild-type mice was  $\sim 4.7$ -fold, which was higher than the difference obtained from in vivo imaging (SI Figure 6g). However, this result is expected since  $A\beta$  antibodies have a much higher sensitivity and specificity for  $A\beta$  species than our chemical imaging probe. In addition, we also conducted high resolution imaging of APP/PS1 mice. As seen in Figure 6d, both hemispheres were clearly outlined with the probe.

**Design of the Inhibitor of Cross-Linking of  $A\beta$  Induced by Copper.** Disruption of brain metal homeostasis during prolonged treatment is an apparent potential side effect of the current metal chelators used for AD therapy,<sup>30,37</sup> because all of the reported chelators are bi- or tridentate ligands for metal ions, and they could coordinate with a metal ion to form an intramolecular complex (Figure 7a,b) before they reach their

targets. It is well-known that copper could coordinate with two imidazoles on H13 and H14 of  $A\beta$  to induce cross-linking at the tyrosine position.<sup>23,25,28,51</sup> A monodentate compound that could specifically interfere with the coordination of imidazoles of H13 and H14 with a metal ion is ideal for avoiding the disruption of metal homeostasis. We hypothesized that placing one imidazole ring around positions H13 and H14 could result in competing and interfering of copper coordination with  $A\beta$ . To accomplish this, we designed the curcumin analogue CRANAD-17 (Figure 7c), in which a curcumin scaffold was used as an anchoring moiety to usher the designed compound to the vicinity of H13 and H14 of  $A\beta$ , and an imidazole ring was introduced into the structure to compete with H13/H14 for copper binding sites.

**In Vitro Spectral Testing of CRANAD-17.** Similar to CRANAD-58, upon mixing with  $A\beta$ , CRANAD-17 displayed fluorescence property changes that resulted in an intensity increase and blue-shift, indicating that this compound could be specific toward  $A\beta$  (red line, Figure 7c). Compared to native  $A\beta$  (blue line, Figure 7c), the intensity of CRANAD-17 was significantly lower upon mixing with [H13R] $A\beta$ , and no significant blue-shift was observed either (blue line, Figure 7c), suggesting that CRANAD-17 specifically interacts with H13 within  $A\beta$ . Moreover, the  $^1\text{H}$  NMR spectrum of the core fragment KLVFF showed apparent changes once the fragment was incubated with CRANAD-17 (Figure 7d), indicating that a specific interaction exists between them. Particularly, the exchangeable proton peaks of K16 were remarkably sharper in the presence of CRANAD-17 than without the ligand, where the spectrum was very broad with no visible peaks.

**In Vitro Anticross-Linking Studies with CRANAD-17.** To investigate whether CRANAD-17 could attenuate copper-induced cross-linking of  $A\beta$ , we first used  $A\beta_{42}$  labeled with fluorescent dye (FAM- $A\beta_{42}$ ) as a model. Compared to traditional SDS-PAGE, the advantages of using dye-conjugated  $A\beta_{42}$  include easy and accurate detection using a fluorescence imaging system. To exclude the attenuation effect caused by the interaction of copper with the diketone moiety of CRANAD-17, we used curcumin as a control compound. To compare the effect of the imidazole ring, CRANAD-58 was also used as a control compound. Due to numerous cross-linked products formed during natural or copper-induced cross-linking, our quantification was based on the remaining amount of FAM- $A\beta_{42}$  monomers (the starting material) on SDS-PAGE gel, which can be visualized with a fluorescence imaging system. It is known that covalent cross-linked  $A\beta$  species could not be dissociated by running an SDS-PAGE gel,<sup>34,52</sup> but other noncovalent aggregated species could be dissociated into monomers. Therefore, more cross-linking would result in a smaller number of monomers, and less cross-linking would keep more monomers intact. After 4 h of incubation of FAM- $A\beta_{42}$  monomers with the compounds copper sulfate and vitamin C (used as an initiator),<sup>53</sup> we found that the intensity of the monomeric  $A\beta$  bands with CRANAD-17, CRANAD-58, and curcumin were 1.68-, 1.16-, and 1.04-fold higher than that of the nontreated group (Figure 8a,b). These results indicated that CRANAD-17 had a significantly higher capacity for attenuating copper-induced cross-linking compared to curcumin and its analogues, primarily due to the interference and competition with copper coordination at the H13 position. Interestingly, we did not find a significant amount of high molecular weight oligomers or protofibrils on the SDS-PAGE gel, probably due to the fast aggregation of  $A\beta_{42}$  after copper



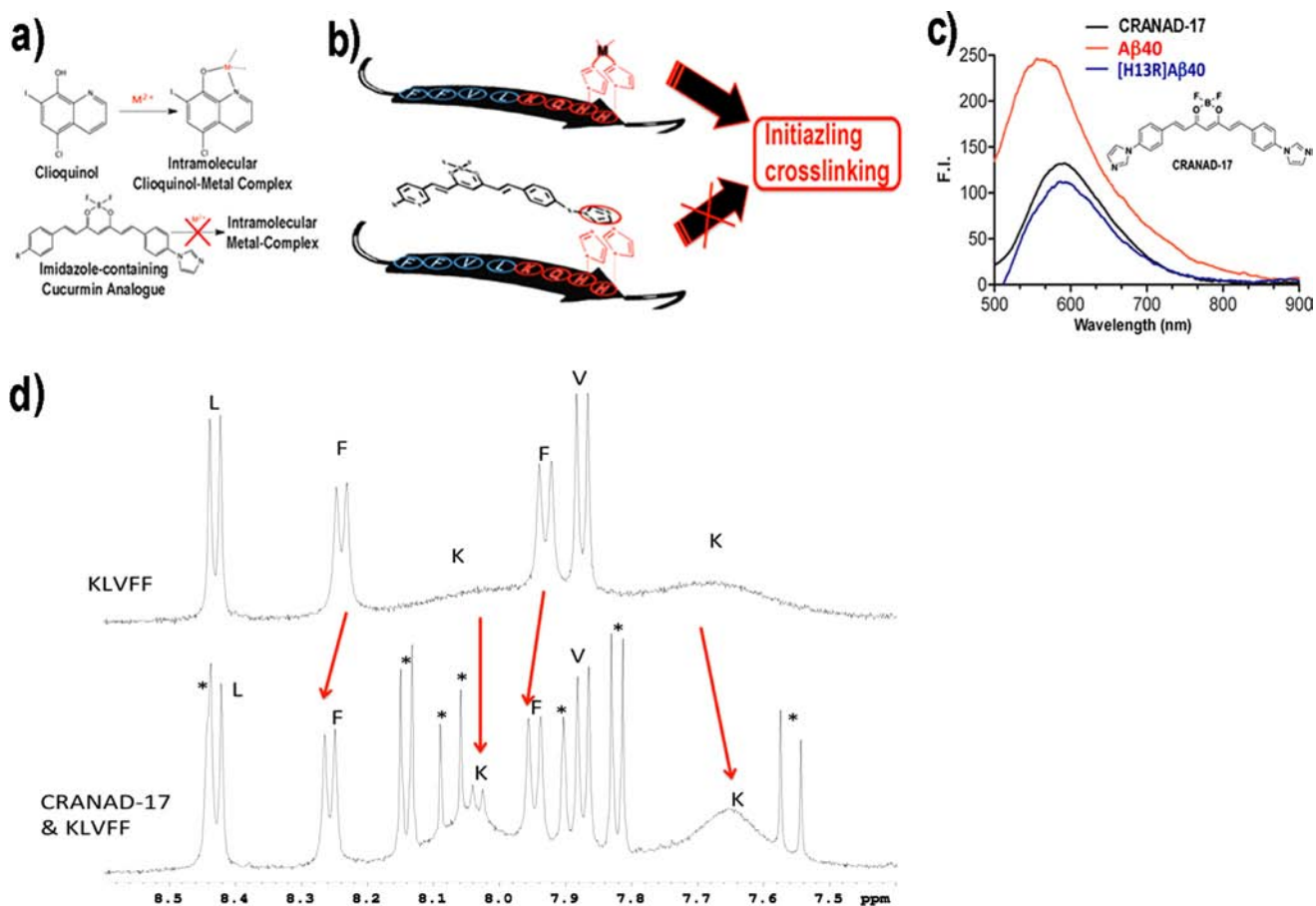


**Figure 7.** (a) Clioquinol, a bidentate ligand for copper, coordinates with copper to form intramolecular complex (top); monodentate compound does not form intramolecular complex with copper. (b) The proposed interaction model between  $A\beta$  (HHQKLVFF segment shown) and the designed imidazole-containing curcumin analogue. (c) Fluorescence spectra of CRANAD-17 alone (black), with  $A\beta$ 40 (red), and with [H13R] $A\beta$ 40 (blue). (d)  $^1\text{H}$  NMR spectra of KLVFF (top) and of KLVFF with CRANAD-17 (bottom). \* Indicated that the peaks originated from ligand CRANAD-17.

treatment, which resulted in the formation of insoluble species that could not enter into the gel.<sup>34</sup>

In addition, it is possible that copper coordination with two imidazole moieties from two CRANAD-17 molecules could lead to the lowering of copper concentration in solution, which thus could result in less cross-linking. To exclude this possibility, 4-(1H-imidazol-1-yl) benzene, which has an imidazole ring for potential copper chelating, was used as a control compound. We found that 4-(1H-imidazol-1-yl) benzene could indeed attenuate cross-linking, but the effect was relatively small compared to CRANAD-17 (Figure 8c and SI Figure 8a), suggesting that nonspecific copper sequestration played only a minor role.

Though FAM- $A\beta$ 42 represents an excellent model for testing our hypothesis, it differs from its native  $A\beta$  counterpart. Therefore, it was necessary to test whether our designed curcumin analogues were able to attenuate native  $A\beta$  cross-linking induced by copper. To this end, we incubated native  $A\beta$ 42 with curcumin, CRANAD-58, and CRANAD-17 under the same conditions as above. Western blot results showed that curcumin, CRANAD-58, and CRANAD-17 could attenuate cross-linking (Figure 8d,e). Similar to the results obtained with FAM- $A\beta$ , CRANAD-17 showed a significantly higher attenuation effect than curcumin and CRANAD-58 (Figure 8d,e), again suggesting that the imidazole ring of CRANAD-17 played a primary role. We also found that the attenuation effect of

CRANAD-17 was concentration dependent (Figure 8f and SI Figure 8b), with the response reaching a plateau at a 5:1 CRANAD-17/ $A\beta$ 42 ratio. Similar to the results obtained with FAM- $A\beta$ 42, no significant amount of high molecular weight species was observed for the groups treated with copper, copper + curcumin, and copper + CRANAD-58. These data most likely indicated that  $A\beta$ 42 could aggregate fast into insoluble species that are too large to enter the gel.<sup>34</sup> We also noticed that  $A\beta$ 42 treated with CRANAD-17/copper showed a certain amount of high molecular weight oligomeric species (Figure 8d, lane 4), suggesting that CRANAD-17 could slow down the aggregation process of  $A\beta$ 42 induced by copper treatment.

To investigate whether CRANAD-17 was able to inhibit the aggregation of  $A\beta$ 42 and to assess the degree of aggregation, we used both TEM and Thioflavin t test. Compared to the control group ( $A\beta$ 42 treated with copper only), we found less visible fibrils in the CRANAD-17 treated group (SI Figure 9a). Additionally, Thioflavin t test showed a lower fluorescence signal after CRANAD-17 treatment (SI Figure 9b), indicating that CRANAD-17 could also reduce  $A\beta$ 42 aggregation.

To further investigate whether CRANAD-17 could reduce the formation of  $A\beta$  fibrils that were formed by aggregating/cross-linking, we used a dot blot to compare the total signal intensity of the dots with and without CRANAD-17. It has been reported that different antibodies have different specificity toward  $A\beta$  species. Murray et al. reported that antibody 2H4

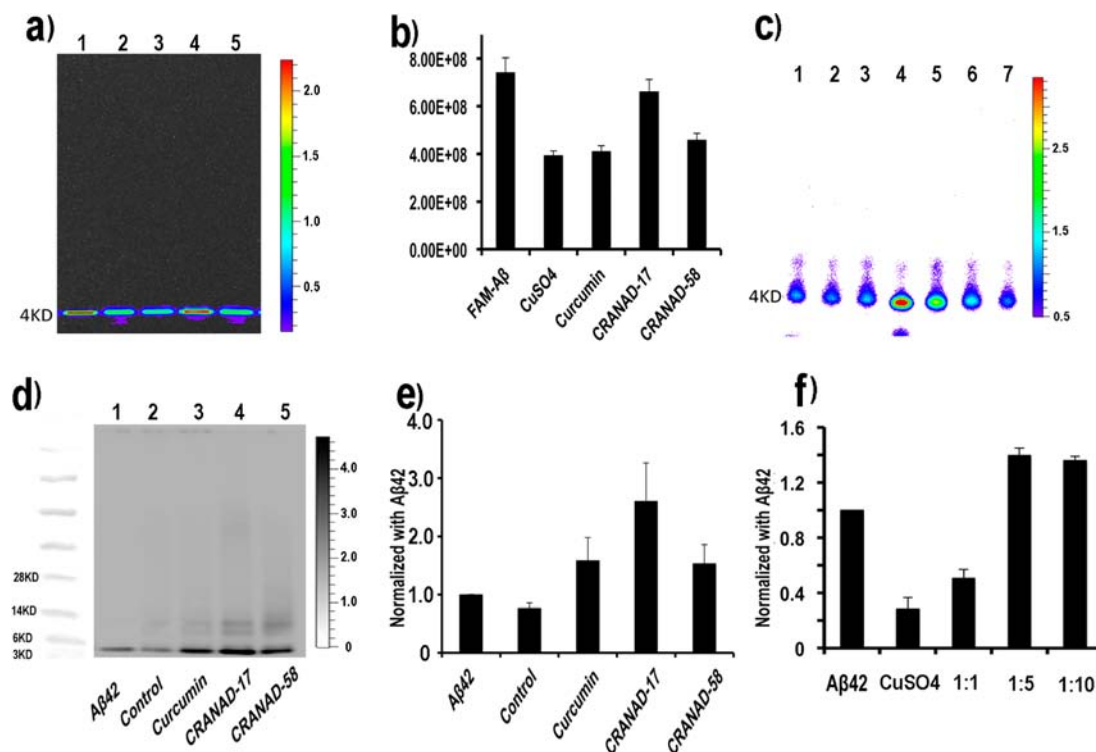


**Figure 8.** SDS-PAGE gel electrophoresis and Western blotting of Aβ<sub>42</sub> species. (a) SDS-PAGE gel of FAM- Aβ<sub>42</sub> alone (lane 1), CuSO<sub>4</sub> (lane 2), CuSO<sub>4</sub> + curcumin (lane 3), CuSO<sub>4</sub> + CRANAD-17 (lane 4), and CuSO<sub>4</sub> + CRANAD-58 (lane 5). (b) Quantitative analysis of the intensities of the monomeric bands in (a). (c) SDS-PAGE gel of FAM- Aβ<sub>42</sub> treated with CuSO<sub>4</sub> + imidazole control (lanes 1–3, ratio FAM- Aβ<sub>42</sub>/imidazole control = 1:10, 1:5, 1:1), CuSO<sub>4</sub> + CRANAD-17 (lanes 4–6, ratio FAM- Aβ<sub>42</sub>/CRANAD-17 = 1:10, 1:5, 1:1), and CuSO<sub>4</sub> only (lane 7). (d) Western blotting of the native Aβ<sub>42</sub> (lane 1), with CuSO<sub>4</sub> (lane 2), CuSO<sub>4</sub> + curcumin (lane 3), CuSO<sub>4</sub> + CRANAD-17 (lane 4), and CuSO<sub>4</sub> + CRANAD-58 (lane 5). (e) Quantitative analysis of the monomeric bands in (d). (f) Dose-dependent study for CRANAD-17. Quantitative analysis of the native Aβ<sub>42</sub> monomeric bands (without copper) with CuSO<sub>4</sub> and with CuSO<sub>4</sub> + CRANAD-17 (Aβ<sub>42</sub>/CRANAD-17 = 1:1, 1:5, and 1:10). The data indicated that the attenuation of copper-induced cross-linking by CRANAD-17 was concentration dependent.

showed better recognizing capability for Aβ fibrils than for other soluble Aβs.<sup>54,55</sup> As expected, the intensity was significantly lower from the dot with CRANAD-17 presence when antibody 2H4 was used (SI Figure 10). This data further supported that CRANAD-17 was effective for reducing Aβ fibril formation.

## DISCUSSION

Although positron emission tomography (PET) imaging has been used for monitoring the efficacy of therapeutic agents for AD in humans, it has rarely been used for monitoring the effectiveness of drug treatment in small animals.<sup>56–61</sup> The most likely reasons include the insensitivity of the imaging probes for Aβ species (particularly for soluble species),<sup>17,62–65</sup> the small amount of total Aβs in the brain of a small animal,<sup>57,58</sup> the complicated experimental procedure and data analysis for small animals, and the high cost of PET probe synthesis and PET imaging. Therefore, a tremendous demand for imaging agents that could be used for monitoring of the effectiveness of the treatments in small animals for preclinical drug development has not been met. Compared to PET imaging, in vivo molecular fluorescence imaging is in principal more suitable for animal studies, due to its low cost, simple operation, and easy data analysis. We believe that CRANAD-58 has the potential to meet the need of monitoring total Aβ concentration changes in small animals.

Several PET and fluorescence imaging probes for amyloid beta have been reported. However, none of them was

originated from a rational design that was based on the unique structural properties of the Aβ peptide. In this report, we successfully designed the imaging probe CRANAD-58 based on the structural stereohindrance compatibility and hydrophilic/hydrophobic property of the HHQKLVFF segment and demonstrated that it was capable of detecting both soluble and insoluble Aβs.

The probe that is capable of only detecting soluble Aβ species is highly desirable for in vivo studies; however, both soluble and insoluble Aβs actually coexist during the disease progression. It is widely believed that the initial stage of pathology is represented by the excessive accumulation of Aβ monomers caused by imbalanced Aβ clearance.<sup>11,12</sup> The early predominance of soluble species gradually shifts to a majority of insoluble species with the progression of AD.<sup>66,67</sup> Therefore, the probe capable of detecting both soluble and insoluble Aβs could have the potential to monitor the changes in Aβs from the very early stages characterized by over accumulation of Aβ monomers, to the late stages highlighted by the presence of dominant insoluble Aβs.

Higher molecular weight Aβs, such as dimers and oligomers, are believed to be more neurotoxic than insoluble Aβs. In this report, we found that our probe detected both toxic species by demonstrating significant fluorescence property changes. However, we also noticed that the fluorescence intensities of CRANAD-58 with dimers and oligomers were lower than that with monomeric and aggregated Aβs. This result most likely suggested that CRANAD-58 was very stereohindrance



sensitive, because the dimers were mutated at S26C and the oligomers may have several different secondary structures.

Our docking experiments were conducted with a segment of  $\beta$ -sheet  $A\beta$  fibril that was extracted from PDB: 2LMO. However, in reality, the structures of  $A\beta$ s are more complicated, while no X-ray structure is available as a template for docking. Furthermore, different  $A\beta$ s may have different secondary structures. Therefore, the results from the docking experiments only partially reflect the actual interaction. In our case, both experimental and docking data indicated that the hydrophobic moiety of  $A\beta$  interacts with the hydrophobic moiety of CRANAD-58, and the hydrophilic segment of  $A\beta$  interacts with the moderately hydrophilic pyridyl moiety of CRANAD-58. However, while our experimental data supported interaction between CRANAD-58 and H13, the docking results were not consistent with this observation. Interestingly, Masuda et al. has recently demonstrated using solid-state NMR studies that curcumin could specifically interact with  $A\beta$  between the regions of V12 and LVFFA ( $A\beta$ 17–21).<sup>68</sup> Our experimental results with docking studies were very similar to their results.

Our results with docking experiments of CRANAD-58 with  $A\beta$  were only partially coherent with our fluorescence experimental data, however it is very challenging to verify the interaction with soluble  $A\beta$ s using NMR techniques due to the following reasons. First, soluble  $A\beta$ s normally exist in transient status, and their conformation could not be fixed during NMR acquisition. Second, high concentrations of  $A\beta$ s are required for NMR studies, which represents a challenge due to rapid aggregation of  $A\beta$ s under these conditions. Third, soluble  $A\beta$  could contain many species that may have very different sizes and structures. Conceivably, it is very difficult to study specific interaction between a small molecule and  $A\beta$ s with different structures. Several groups have performed excellent research with insoluble fibrillar  $A\beta$ s using various NMR techniques.<sup>28,43,47,68–81</sup> In the near future, we will employ different techniques including NMR to elucidate the interaction between CRANAD-58 and fibrillar  $A\beta$ s.

We demonstrated that CRANAD-58 was able to differentiate transgenic APP/PS1 and wild-type mice that were as young as 4 months old. At this age no obvious  $A\beta$  plaques could be observed, and the majority of  $A\beta$  species most likely existed in soluble form. It has been reported that at this age the APP/PS1 mice are behaviorally normal, suggesting that monomeric  $A\beta$  are the dominant species. In fact, the initial stage of AD is highlighted by an overaccumulation of monomeric  $A\beta$ s, which slowly aggregate into oligomers and insoluble fibrils and plaques. We believe that CRANAD-58 may be a potential probe for monitoring  $\beta$ -amyloid species at an early/presymptomatic stage. However, it is technically challenging to directly validate the interaction between CRANAD-58 and soluble  $A\beta$  species in vivo or ex vivo, because currently available microscopes do not have a high enough resolution to see the morphology of the soluble species, which are normally <100 nm in size.

Developing imaging probes and therapeutics have certain similar requirements, such as specificity for ligands.<sup>22</sup> In this report, we first demonstrated that the imaging probe CRANAD-58 had a certain specificity toward  $A\beta$ s. Based on the interaction mechanism studies, we designed a potential therapeutic agent by utilizing the specificity of the curcumin scaffold for  $A\beta$ s. Currently, developing aggregation inhibitors of  $A\beta$  is still one very active direction in AD drug development.

It is well-known that the  $A\beta$  aggregation process could be divided into two categories: reversible aggregation due to physical hydrophobic stacking and irreversible aggregation due to covalent cross-linking.<sup>82,83</sup> Various aggregation inhibitors or promoters of  $A\beta$  have been intensively studied;<sup>84–98</sup> however, only few have been suggested to have specificity toward cross-linking inhibition.<sup>99,100</sup> In addition, most of the discovered anti-aggregation agents are not based on a specific interaction mechanism; instead, these compounds were selected using high-throughput screening or other approaches.<sup>92–94</sup> Therefore, their specific interaction mechanisms are not clear. In this report, we have designed imidazole-containing curcumin analogues to specifically interrupt the coordination of copper and imidazoles from H13 and H14. We believe that our study opens a new possibility for designing new drugs for AD based on the specific interaction mechanism.

Studies utilizing CRANAD-58 for monitoring the progression of the disease as well as for drug treatment in mice are currently undergoing in our group. Although application of CRANAD-58 for translational clinical studies is hardly possible due to the limitations imposed by optical imaging, adapting CRANAD-58 into a PET probe is a promising approach. Translation from mice to human is always challenging; however, several very successful examples have been established in the field of PET imaging of  $A\beta$ s.<sup>56</sup> Interestingly, several probes including PiB have failed to image  $A\beta$ s in a transgenic mouse model before entering into clinical studies,<sup>57,58,101</sup> even though transgenic mice have a much higher concentration of  $A\beta$ s (based on the weight of tissue) than AD patients (the difference is up to 2 orders of magnitude for both soluble and insoluble  $A\beta$ s).<sup>101,102</sup> We believe that incorporation of PET isotopes into the CRANAD-58 molecule could be feasible for the following translational studies.

## EXPERIMENT

Reagents used for the synthesis were purchased from Aldrich and used without further purification. The pH of the PBS buffer was 7.4. Column chromatography was performed on silica gel (SiliCycle Inc., 60 Å, 40–63 mm) slurry packed into glass columns. Synthetic  $A\beta$  peptide (1–40/42) and amylin were purchased from rPeptide (Bogart, GA, 30622). Synthetic S26C  $A\beta$  dimer was purchased from AnaSpec. Aggregates for in vitro studies were generated by the slow stirring of  $A\beta$ 40 in PBS buffer for 3 days at room temperature. CRANAD-2, and -6, -17, -23, -54, and -58 were dissolved in DMSO to prepare a 25.0  $\mu$ M stock solution. <sup>1</sup>H and <sup>13</sup>C NMR spectra were recorded at 500 and 125 MHz, respectively, and reported in ppm downfield from tetramethylsilane. Fluorescence measurements were carried out using an F-4500 fluorescence spectrophotometer (Hitachi). Mass spectra were obtained at Harvard University, Department of Chemistry Instrumentation Facility. Transgenic female APP-PS1 mice and age-matched wild-type female mice were purchased from Jackson Laboratory. All animal experiments were approved by the Institutional Animal Use and Care Committee at Massachusetts General Hospital.

**Synthesis of CRANAD-2, -6, -17, -23, -54, and -58.** CRANAD-2. The synthesis was performed according to our previously reported procedure.<sup>20,38</sup>

CRANAD-6. The synthesis was performed according to the modified protocol of our previously reported procedure.<sup>38</sup> 2,2-difluoro-1,3-dioxaboryl-pentadione was synthesized using a modified procedure.<sup>38</sup> The 2,2-difluoro-1,3-dioxaboryl-pentadione crystals (0.15g, 0.1 mmol) were dissolved in acetonitrile (3.0 mL), followed by the additions of acetic acid (0.2 mL), tetrahydroisoquinoline (0.04 mL, 0.3 mmol), and 4-*N,N'*-dimethylamino-1-naphthaldehyde (0.40g, 2.0 mmol). The resulting solution was stirred at 60 °C overnight. A black residue obtained after removing the solvent was subjected to flash column chromatography with methylene chloride to give a black powder (yield

15.0%).  $^1\text{H}$  NMR ( $\text{CDCl}_3$ )  $\delta$ (ppm) 2.98 (s, 12H), 6.10 (s, 1H), 6.75 (d, 2H,  $J = 15.0$  Hz), 6.98 (d, 2H,  $J = 7.5$  Hz), 7.51 (t, 2H,  $J = 7$  Hz), 7.58 (t, 2H,  $J = 7$  Hz), 7.85 (d, 2H,  $J = 7.5$  Hz), 8.16 (d, 2H,  $J = 8.0$  Hz), 8.27 (d, 2H,  $J = 8.0$  Hz), 8.83 (d, 2H,  $J = 15.0$  Hz).  $^{13}\text{C}$  NMR ( $\text{CDCl}_3$ )  $\delta$ (ppm) 44.6, 102.2, 113.0, 119.4, 123.6, 124.6, 125.30, 125.38, 127.2, 127.3, 127.7, 133.4, 142.9, 155.2, 178.6.  $^{19}\text{F}$  NMR ( $\text{CDCl}_3$ )  $\delta$ (ppm) 140.933, 140.993. ESI-MS ( $M - H$ )  $m/z = 510.30$ .

**CRANAD-17.** The 2,2-difluoro-1,3-dioxaboryl-pentadione crystals (80 mg, 0.5 mmol) were dissolved in acetonitrile (4.0 mL), followed by the additions of acetic acid (0.1 mL), tetrahydroisoquinoline (20  $\mu\text{L}$ ), and 4-(1H-imidazol-1-yl)benzaldehyde (172 mg, 1 mmol). The resulted solution was stirred at 60 °C for 4 h. An orange solid was obtained after filtrating the reaction mixture, and the solid was washed with EtOAc to give a dark orange powder CRANAD-17, 46 mg, yield 20%.  $^1\text{H}$  NMR ( $\text{DMSO}-d_6$ )  $\delta$ (ppm) 6.63(s, 1H), 7.14(s, 2H), 7.31 (d, 2H,  $J = 15.5$  Hz), 7.82 (d, 4H,  $J = 8.5$  Hz), 7.88 (s, 2H), 8.03 (d, 4H,  $J = 8.5$  Hz), 8.08 (d, 2H,  $J = 15.5$  Hz), 8.43 (s, 2H).  $^{13}\text{C}$  NMR ( $\text{DMSO}-d_6$ )  $\delta$ (ppm) 102.99, 118.15, 120.73, 121.98, 130.71, 131.79, 132.82, 136.10, 139.60, 146.15, 180.35.  $^{19}\text{F}$  NMR ( $\text{DMSO}-d_6$ )  $\delta$ (ppm) 137.069, 137.129. ESI-MS ( $M - H$ )  $m/z = 458.2$ .

**CRANAD-23.** The synthesis followed the similar procedure as for CRANAD-6.  $^1\text{H}$  NMR ( $\text{CDCl}_3$ )  $\delta$ (ppm) 4.00(s, 4H), 6.61(s, 1H), 7.31(d, 2H,  $J = 15$  Hz), 7.37(dd, 2H,  $J_1 = 7.5$  Hz,  $J_2 = 7.5$  Hz), 7.42(dd, 2H,  $J_1 = 7.5$  Hz,  $J_2 = 7.5$  Hz), 7.63(d, 2H,  $J = 7.5$  Hz), 7.91(d, 2H,  $J = 8$  Hz), 7.99(d, 2H,  $J = 7.5$  Hz), 8.03(d, 2H,  $J = 8$  Hz), 8.11(d, 2H,  $J = 15$  Hz), 8.12(s, 2H).  $^{13}\text{C}$  36.83, 121.10, 121.21, 121.37, 125.76, 126.29, 127.51, 128.46, 129.76, 133.31, 140.64, 144.38, 144.72, 145.54, 147.49, 180.18.  $^{19}\text{F}$  NMR ( $\text{CDCl}_3$ )  $\delta$ (ppm) 137.37, 137.43. ESI-MS:  $m/z$ :  $[M + H]^+$  453.2.

**CRANAD-54.** 2,2-Difluoro-1,3-dioxaboryl-pentadione crystals (0.15g, 1.0 mmol) were dissolved in acetonitrile (2.0 mL), followed by the additions of acetic acid (0.1 mL), tetrahydroisoquinoline (0.02 mL, 0.15 mmol), and 4-(dimethylamino)-benzaldehyde (0.15g, 1.0 mmol). The resulting solution was stirred at 60 °C overnight. A black residue was obtained after removing the solvent and further purified with flash column chromatography (hexane:ethyl acetate = 5:1) to give a red powder CRANAD-54 (yield 20.0%).  $^1\text{H}$  NMR ( $\text{CDCl}_3$ )  $\delta$ (ppm) 2.24 (s, 3H), 3.08 (s, 6H), 5.88 (s, 1H), 6.38 (d, 1H,  $J = 15.0$  Hz), 6.66 (d, 2H,  $J = 9.0$  Hz), 7.48 (d, 2H,  $J = 9.0$  Hz), 8.10 (d, 1H,  $J = 15.0$  Hz).  $^{13}\text{C}$  NMR ( $\text{CDCl}_3$ )  $\delta$ (ppm) 23.87, 40.07, 100.41, 111.90, 113.08, 121.58, 132.14, 150.02, 153.31, 180.66, 186.90.  $^{19}\text{F}$  NMR ( $\text{CDCl}_3$ )  $\delta$ (ppm) 140.38, 140.44. ESI-MS ( $2M - H$ )  $m/z = 559.3$ .

**CRANAD-58.** 6-(Diethylamino)-3-pyridinylaldehyde (18 mg, 0.1 mg) and CRANAD-54 (30 mg, 0.1 mmol) were dissolved in acetonitrile (1.0 mL), followed by the addition of acetic acid (20  $\mu\text{L}$ ) and tetrahydroisoquinoline (4  $\mu\text{L}$ , 0.03 mmol). The resulting solution was stirred at 60 °C overnight. A black residue was obtained after removing the solvent and further purified with flash column chromatography (hexane:ethyl acetate:CH<sub>2</sub>Cl<sub>2</sub> = 2:1:1) to give a dark powder CRANAD-58 (yield 13.6%).  $^1\text{H}$  NMR ( $\text{CDCl}_3$ )  $\delta$ (ppm) 1.15 (t, 6H,  $J = 7.0$  Hz), 2.98 (s, 6H), 3.50 (q, 4H,  $J = 7.0$  Hz), 5.79 (s, 1H), 6.31 (d, 1H,  $J = 15.5$  Hz), 6.35 (d, 1H,  $J = 15.0$  Hz), 6.42 (d, 1H,  $J = 9.5$  Hz), 6.57 (d, 2H,  $J = 8.5$  Hz), 7.39 (d, 2H,  $J = 8.5$  Hz), 7.57 (dd, 1H,  $J = 2.5$ , 9.5 Hz), 7.78 (d, 1H,  $J = 15.0$  Hz), 7.85 (d, 1H,  $J = 15.5$  Hz), 8.22 (d, 1H,  $J = 2.5$  Hz).  $^{13}\text{C}$  NMR ( $\text{CDCl}_3$ )  $\delta$ (ppm) 12.95, 40.07, 43.05, 101.01, 106.09, 111.87, 114.75, 115.27, 118.35, 122.24, 131.55, 135.48, 143.60, 147.27, 152.70, 152.76, 158.51, 177.35, 178.32.  $^{19}\text{F}$  NMR ( $\text{CDCl}_3$ )  $\delta$ (ppm) 141.93, 141.99. ESI-MS ( $M - H$ )  $m/z = 440.3$ .

**A $\beta$ 40/42 Monomer Preparation.** A $\beta$ 40/42 monomers were prepared by further purification of commercially available A $\beta$ 40/42 peptide (rPeptide, catalogue no. A-1153-1 and A-1163-1 with HFIP treatment) using HPLC. Purified monomers were stored as powder/film or in hexafluoroisopropanol (HFIP) as stock solutions.<sup>103</sup> Particle size measurement was conducted using Zetasizer Nano (Malvern, Worcestershire, U.K.). Ten microliters of A $\beta$ 40 monomer (25  $\mu\text{M}$ ) in HFIP were dried with argon gas and then reconstituted in 1.0 mL of distilled water. The resulting water solution showed no presence of measurable particles as determined by particle size measurements (not shown). TEM results (SI Figure 1a–d), size exclusive chromatography

(SEC) (SI Figure 1e–f), and SDS-GEL (SI Figure 1f) suggested that they were not oligomerized or aggregated. SDS electrophoresis of monomeric A $\beta$ 40/42 peptides was performed using a 4–20% gradient Tris gel (Bio-Rad) and SeeBlueplus2 (Invitrogen)(4-250KD) as a molecular weight marker. A 10  $\mu\text{L}$  sample (2.5  $\mu\text{M}$ ) was loaded, and Tris-glycine buffer was used for running the gel.

**A $\beta$  dimers.** The dimers of S26C A $\beta$ 40 were purchased from AnaSpec.

**A $\beta$ 42 oligomers preparation.** The preparation was performed according to Kayed's reported procedure<sup>44</sup> and confirmed by TEM.

**A $\beta$ 40 aggregate preparation.** A $\beta$ 40 peptide (1.0 mg) was resuspended in 1% ammonia hydroxyl solution (1.0 mL). One hundred microliters of the resulting solution was diluted 10-fold with PBS buffer (pH 7.4) and stirred at room temperature for 3 days. TEM confirmed the formation of aggregates (SI Figure 1).

**TEM Measurement.** Five microliters of 250 nM of an A $\beta$ 40 PBS solution, which was prepared from HFIP stock solution (25  $\mu\text{M}$ ), was dropped to a Formvar coated TEM grid, followed by the addition of 2  $\mu\text{L}$  of a PTA contrast solution to the grid. After 1 min, the liquid on the grid was carefully dried with a corner of filter paper, and the resulting grid was further dried in the air for 2–5 min. The TEM images were obtained with a JEOL 1011 electron microscope. A similar procedure was used for the incubated solution of CRANAD-17 (10  $\mu\text{M}$ ) and A $\beta$ 42 (2.5  $\mu\text{M}$ ).

**Size Exclusion Chromatography.** A 50  $\mu\text{L}$  sample of A $\beta$ 40 monomers (25.0  $\mu\text{M}$ ) in HFIP stock solution was dried with a Speedvac, and the resulting thin film was dissolved with 250  $\mu\text{L}$  PBS. The solution was injected into a SEC system (AKTA system, GE Health) and eluted with ammonia acetate (50 mM pH 8.5, 0.5 mL/min) on a Superdex 75 column. Standard solutions of 43KD, 29KD, 13.5KD, and 6.5KD proteins were also tested under the same condition.

**Fluorescence Spectral Testing of CRANAD-X (X = 2, 6, 17, 23, 54, and 58) with A $\beta$ s.** To test interactions of CRANAD-58 with A $\beta$  species, we utilized the following procedure. Step 1: 1.0 mL of PBS buffer was added to a quartz cuvette as a blank control and its fluorescence was recorded with the same parameters as for CRANAD-58. Step 2: fluorescence of a CRANAD-58 solution (1.0 mL, 250 nM) was recorded with excitation at 610 nm and emission from 630 to 900 nm. Step 3: to the above CRANAD-58 solution, 10  $\mu\text{L}$  of A $\beta$  species (25  $\mu\text{M}$  stock solution in 30% trifluoroethanol or HFIP for monomers and dimers, and 25  $\mu\text{M}$  stock solution in PBS buffer or double distilled water for oligomers and A $\beta$ 40 aggregates) was added to make the final A $\beta$  concentration of 250 nM. Fluorescence readings from this solution were recorded as described in Step 2. The final spectra from steps 2 and 3 were corrected using the blank control from Step 1.

**NMR Studies with KLVFF Segment.**  $^1\text{H}$  NMR spectrum of DMSO- $d_6$  solution of KLVFF (2.0 mM) was recorded at 310 °C followed by addition of 0.96 mg CRANAD-58 (2.0 mM). The resulting solution was kept at room temperature overnight and then subjected to  $^1\text{H}$  NMR spectrum recording at 310 °C. Similar procedure was used for CRANAD-17. The ppm reference peaks were set at 2.49 ppm with DMSO- $d_6$  as the reference.

**Molecular Modeling.** A segment of  $\beta$ -sheet A $\beta$  fibril was extracted from RCSB Protein Data Bank (PDB ID: 2LMO). CRANAD-58 was generated using Sybyl program (Sybyl, version 7.0). The coordination bonds in the molecules were treated as single bonds, thus the atom and bond properties of boron and oxygen were redefined. Gasteiger–Hückel charge was used, and the conformations were minimized using default parameters.

The docking was performed using Glide program (Glide, version 5.5). The  $\beta$ -sheet A $\beta$  was processed by minimal minimization with OPLS2005 force field. The grid was sized to 15 Å in each direction at the center of the HHQKLVFF segment. The two compounds were prepared for docking using Ligprep, and the pH was set as 7.0  $\pm$  2.0 using Epik ionization. The maximum number of low-energy ring conformations was set to 10 per ligand. Ligand docking was performed in SP mode and flexible option, with up to 100 poses saved per molecule. Glide score was consulted for results analyzing.



**Brain Phantom Studies.** A 4 month wild-type (B6C3F1/J) mouse was perfused and sacrificed, and its brain was dissected. The brain was divided into two even halves and put into two eppendorf tubes. Of the two tubes, one contained 50 ng A $\beta$ 42 monomers that were obtained from evaporating 20  $\mu$ L HFIP A $\beta$ 42 monomer solution (2.5  $\mu$ M), and another one was used as the control. To the previous two tubes, 10  $\mu$ L CRANAD-58 (2.5  $\mu$ M in DMSO) and 200  $\mu$ L PBS were added to each tube, and brain tissue blocks were homogenized. The resulting two tubes were imaged with EX/EM = 640/700 nm on IVISSpectrum imaging system. For the oligomers, a similar procedure was used, except oligomers were prepared in PBS or distilled water.

**In Vivo NIR Imaging.** In vivo NIR imaging was performed using IVISSpectrum animal imaging system (Caliper LifeSciences, Perkin-Elmer, Hopkinton, MA). Images were acquired with a 640 nm excitation filter and a 700 nm emission filter. Data analysis was performed using LivingImage 4.2.1 software.

The 4 month old mice (female transgenic APP-PS1,  $n = 3-4$  and age-matched female wild-type control mice,  $n = 3-4$ ) were shaved before background imaging. An injection solution of CRANAD-58 (2.0 mg/kg) was freshly prepared in 20% DMSO, 20% cremorphor, and 60% PBS, and the solution was stabilized for 20 min before injection. Each mouse was injected intravenously with 100  $\mu$ L of CRANAD-58. Fluorescence signals from the brain were recorded before and 5, 10, 30, 60, 120, and 240 min after intravenous injection of the probe. To evaluate our imaging results, an ROI was drawn around the brain region.  $P$  values were calculated using Student  $t$  test.

**ELISA Assay.** The levels of A $\beta$  in the brains were determined using ELISA protocols described previously.<sup>104,105</sup> After imaging, the mice were sacrificed, and their brains were dissected. A half of the brain was homogenized in Tris-buffered saline (TBS) containing protease inhibitors. Extracts were spun at 50 000  $\times g$  for 60 min at 4  $^{\circ}$ C. The A $\beta$  levels were measured using the Wako A $\beta$  ELISA kit according to the provided protocol.<sup>104,105</sup>

**Histological Staining of Brain Slice.** A 30  $\mu$ m brain slice from an 18 month old APP/PS1 mouse was incubated with 1% CRANAD-58 solution (20% ethanol and 80% dd water) for 15 min and then washed with 20% ethanol followed by washing with dd water. Next, the slice was co-stained with 1% Thioflavin T (30% ethanol solution) and covered with VectaShield mounting media. Fluorescence images were observed using Nikon Eclipse 50i microscope.

**Gel Electrophoresis and Western Blotting.** Samples were separated on 4–20% gradient Tris-glycine mini gels (Invitrogen). For FAM-A $\beta$ 42 gels, the images were acquired on IVISSpectrum (Caliper, Perkin-Elmer) with excitation = 465 nm and emission = 520 nm. For native A $\beta$ 42 gels, the gel was transferred to a nitrocellulose membrane in a cooled transferring buffer, and the membrane was blocked at room temperature for 2 h. After blocking, the membrane was incubated in a solution of 6E10 anti-A $\beta$  primary antibody (1:2000 dilution, Covance, Dedham, MA) at 4  $^{\circ}$ C overnight. After washing with TBS buffer, the membrane was incubated with the secondary antibody for 1 h at room temperature. Western Breeze Chemiluminescent kit (Invitrogen) was used to visualize the bands. The images were acquired using IVISSpectrum (Caliper, Perkin-Elmer) using bioluminescence imaging setting. SeeBlueplus2 (Invitrogen)(4-250KD) was used as a molecular weight marker. For dot blot, the reported procedure was followed.<sup>55</sup> The samples were dropped to a nitrocellulose membrane and dried at room temperature for 1 h, then a Western blot was performed. The 2H4 antibody was used instead of 6E10.

All the samples used for SDS-PAGE gel, Western blot, and dot blot were prepared using the same procedure as described below. A 5  $\mu$ L HFIP (hexafluoroisopropanol) solution (25  $\mu$ M) of native A $\beta$ 42 or FAM-A $\beta$ 42 was added to a 1.5 mL eppendorf tube. After evaporating the organic solvent under vacuum, a 5  $\mu$ L DMSO or DMSO solution of CRANAD-17 (100  $\mu$ M) was added to the tube, followed by the addition of 15  $\mu$ L of vitamin C solution in PBS (33.3  $\mu$ M) and 5  $\mu$ L of copper sulfate solution in PBS (pH 7.4) (12.5  $\mu$ M). The resulting mixture was incubated at 37  $^{\circ}$ C for 4 h and then subjected to gel electrophoresis. For dose dependency study, 5  $\mu$ L of DMSO solution of different CRANAD-17 concentrations (25, 125, 250  $\mu$ M) was added to obtain CRANAD-17/A $\beta$ 42 ratio equals 1:1, 5:1, and 10:1.

**Thioflavin T test.** A 2.5  $\mu$ M of A $\beta$ 42 solution in PBS (pH 7.4) was placed at 37  $^{\circ}$ C for 24 h, and 10  $\mu$ L of this solution was added to 1.0 mL PBS solution. The resulting solution was then subjected to fluorescence spectrum recording with excitation = 440 nm and emission = 470–800 nm (baseline recording). To this solution, 10  $\mu$ L of Thioflavin T (2.5  $\mu$ M in PBS (pH 7.4)) was added, and the spectrum was recorded. The quantification was conducted at  $\lambda_{em} = 500$  nm for Thioflavin T reading by subtracting the baseline reading. For CRANAD-17 (10  $\mu$ M) incubation, the quantification was conducted by subtracting the readings at baseline and CRANAD-17 at  $\lambda_{em} = 500$  nm.

## ■ ASSOCIATED CONTENT

### ● Supporting Information

Supplemental Figures 1–10. This material is available free of charge via the Internet at <http://pubs.acs.org>.

## ■ AUTHOR INFORMATION

### Corresponding Authors

[cran@nmr.mgh.harvard.edu](mailto:cran@nmr.mgh.harvard.edu)

[amoore@helix.mgh.harvard.edu](mailto:amoore@helix.mgh.harvard.edu)

### Notes

The authors declare no competing financial interest.

## ■ ACKNOWLEDGMENTS

This work was supported by K25AG036760 award to C.R. The authors would also like to thank Alana Ross and Pamela Pantazopoulos, B.S. for proofreading this manuscript.

## ■ REFERENCES

- (1) Selkoe, D. J. *Nat. Med.* **2011**, *17*, 1060.
- (2) Jakob-Roetne, R.; Jacobsen, H. *Angew. Chem., Int. Ed. Engl.* **2009**, *48*, 3030.
- (3) Gravit, L. *Nature* **2011**, *475*, S9.
- (4) Holtzman, D. M.; Mandelkow, E.; Selkoe, D. J. *Cold Spring Harbor Perspect. Med.* **2012**, *2*; pii: a011585.
- (5) McLean, C. A.; Cherny, R. A.; Fraser, F. W.; Fuller, S. J.; Smith, M. J.; Beyreuther, K.; Bush, A. I.; Masters, C. L. *Ann. Neurol.* **1999**, *46*, 860.
- (6) Lue, L. F.; Kuo, Y. M.; Roher, A. E.; Brachova, L.; Shen, Y.; Sue, L.; Beach, T.; Kurth, J. H.; Rydel, R. E.; Rogers, J. *Am. J. Pathol.* **1999**, *155*, 853.
- (7) Terry, R.; Masliah, E.; Salmon, D. P.; Butters, N.; DeTeresa, R.; Hill, R.; Hansen, L. A.; Katzman, R. *Ann. Neurol.* **1991**, *30*, 572.
- (8) Haass, C.; Selkoe, D. J. *Nat. Rev. Mol. Cell Biol.* **2007**, *8*, 101.
- (9) Walsh, D. M.; Selkoe, D. J. *J. Neurochem.* **2007**, *101*, 1172.
- (10) Shankar, G. M.; Li, S.; Mehta, T. H.; Garcia-Munoz, A.; Shepardson, N. E.; Smith, I.; Brett, F. M.; Farrell, M. A.; Rowan, M. J.; Lemere, C. A.; Regan, C. M.; Walsh, D. M.; Sabatini, B. L.; Selkoe, D. J. *Nat. Med.* **2008**, *14*, 837.
- (11) Hardy, J.; Selkoe, D. J. *Science* **2002**, *297*, 353.
- (12) Mawuenyega, K. G.; Sigurdson, W.; Ovod, V.; Munsell, L.; Kasten, T.; Morris, J. C.; Yarasheski, K. E.; Bateman, R. J. *Science* **2011**, *330*, 1774.
- (13) Klunk, W. E. *Neurobiol. Aging* **2011**, *32*, S20.
- (14) Chang, W. M.; Dakanali, M.; Capule, C. C.; Sigurdson, C. J.; Yang, J.; Theodorakis, E. A. *ACS Chem. Neurosci.* **2011**, *2*, 249.
- (15) Choi, S. R.; Golding, G.; Zhuang, Z.; Zhang, W.; Lim, N.; Hefti, F.; Benedum, T. E.; Kilbourn, M. R.; Skovronsky, D.; Kung, H. F. *J. Nucl. Med.* **2009**, *50*, 1887.
- (16) Li, Q.; Lee, J. S.; Ha, C.; Park, C. B.; Yang, G.; Gan, W. B.; Chang, Y. T. *Angew. Chem., Int. Ed.* **2004**, *43*, 6331.
- (17) Hintersteiner, M.; Enz, A.; Frey, P.; Jatou, A. L.; Kinzy, W.; Kneuer, R.; Neumann, U.; Rudin, M.; Staufenberg, M.; Stoekli, M.; Wiederhold, K. H.; Gremlich, H. U. *Nat. Biotechnol.* **2005**, *23*, 577.
- (18) Cui, M.; Ono, M.; Kimura, H.; Liu, B.; Saji, H. *J. Med. Chem.* **2011**, *54*, 2225.



- (19) Ono, M.; Watanabe, H.; Kimura, H.; Saji, H. *ACS Chem. Neurosci.* **2012**, *3*, 319.
- (20) Ran, C.; Zhao, W.; Moir, R. D.; Moore, A. *PLoS One* **2011**, *6*, e19362.
- (21) LeVine, H., III. *Arch. Biochem. Biophys.* **2002**, *404*, 106.
- (22) Vallabhajosula, S. *Molecular imaging: radiopharmaceuticals for PET and SPECT*; Springer-Verlag: Berlin, 2009.
- (23) Atwood, C. S.; Perry, G.; Zeng, H.; Kato, Y.; Jones, W. D.; Ling, K. Q.; Huang, X.; Moir, R. D.; Wang, D.; Sayre, L. M.; Smith, M. A.; Chen, S. G.; Bush, A. I. *Biochemistry* **2004**, *43*, 560.
- (24) Noy, D.; Solomonov, I.; Sinkevich, O.; Arad, T.; Kjaer, K.; Sagi, I. *J. Am. Chem. Soc.* **2008**, *130*, 1376.
- (25) Streltsov, V. A.; Titmuss, S. J.; Epa, V. C.; Barnham, K. J.; Masters, C. L.; Varghese, J. N. *Biophys. J.* **2008**, *95*, 3447.
- (26) Himes, R. A.; Park, G. Y.; Siluvai, G. S.; Blackburn, N. J.; Karlin, K. D. *Angew. Chem.* **2008**, *47*, 9084.
- (27) Lu, Y.; Prudent, M.; Qiao, L.; Mendez, M. A.; Girault, H. H. *Metallomics* **2010**, *2*, 474.
- (28) Parthasarathy, S.; Long, F.; Miller, Y.; Xiao, Y.; McElheny, D.; Thurber, K.; Ma, B.; Nussinov, R.; Ishii, Y. *J. Am. Chem. Soc.* **2011**, *133*, 3390.
- (29) Lannfelt, L.; Blennow, K.; Zetterberg, H.; Batsman, S.; Ames, D.; Harrison, J.; Masters, C. L.; Targum, S.; Bush, A. I.; Murdoch, R.; Wilson, J.; Ritchie, C. W. *Lancet Neurol.* **2008**, *7*, 779.
- (30) White, A. R.; Barnham, K. J.; Bush, A. I. *Expert Rev. Neurother.* **2006**, *6*, 711.
- (31) Faux, N. G.; Ritchie, C. W.; Gunn, A.; Rembach, A.; Tsatsanis, A.; Bedo, J.; Harrison, J.; Lannfelt, L.; Blennow, K.; Zetterberg, H.; Ingelsson, M.; Masters, C. L.; Tanzi, R. E.; Cummings, J. L.; Herd, C. M.; Bush, A. I. *J. Alzheimer's Dis.* **2010**, *20*, 509.
- (32) Duce, J. A.; Bush, A. I. *Prog. Neurobiol.* **2010**, *92*, 1.
- (33) Choi, J. S.; Braymer, J. J.; Nanga, R. P.; Ramamoorthy, A.; Lim, M. H. *Proc. Natl. Acad. Sci. U.S.A.* **2010**, *107*, 21990.
- (34) Sharma, A. K.; Pavlova, S. T.; Kim, J.; Finkelstein, D.; Hawco, N. J.; Rath, N. P.; Mirica, L. M. *J. Am. Chem. Soc.* **2012**, *134*, 6625.
- (35) Rodriguez-Rodriguez, C.; Sanchez de Groot, N.; Rimola, A.; Alvarez-Larena, A.; Lloveras, V.; Vidal-Gancedo, J.; Ventura, S.; Vendrell, J.; Sodupe, M.; Gonzalez-Duarte, P. *J. Am. Chem. Soc.* **2009**, *131*, 1436.
- (36) Hindo, S. S.; Mancino, A. M.; Braymer, J. J.; Liu, Y.; Vivekanandan, S.; Ramamoorthy, A.; Lim, M. H. *J. Am. Chem. Soc.* **2009**, *131*, 16663.
- (37) Schafer, S.; Pajonk, F. G.; Multhaup, G.; Bayer, T. A. *J. Mol. Med. (Berlin)* **2007**, *85*, 405.
- (38) Ran, C.; Xu, X.; Raymond, S. B.; Ferrara, B. J.; Neal, K.; Bacskai, B. J.; Medarova, Z.; Moore, A. *J. Am. Chem. Soc.* **2009**, *131*, 15257.
- (39) Marini, A. M.-L., A.; Biancardi, A.; Mennucci, B. *J. Phys. Chem. B* **2010**, *114*, 17128.
- (40) Caputo, G.; London, E. *Biochemistry* **2003**, *42*, 3275.
- (41) Biancalana, M.; Koide, S. *Biochim. Biophys. Acta* **2010**, *1804*, 1405.
- (42) Hanyu, M.; Ninomiya, D.; Yanagihara, R.; Murashima, T.; Miyazawa, T.; Yamada, T. *J. Pept. Sci.* **2005**, *11*, 491.
- (43) Rzepecki, P.; Schrader, T. *J. Am. Chem. Soc.* **2005**, *127*, 3016.
- (44) Kaye, R.; Head, E.; Thompson, J. L.; McIntire, T. M.; Milton, S. C.; Cotman, C. W.; Glabe, C. G. *Science* **2003**, *300*, 486.
- (45) Marshall, K. E.; Serpell, L. C. *Biochem. Soc. Trans.* **2009**, *37*, 671.
- (46) Hamley, I. W. *Angew. Chem., Int. Ed. Engl.* **2007**, *46*, 8128.
- (47) Krysmann, M. J.; Castelletto, V.; Kelarakis, A.; Hamley, I. W.; Hule, R. A.; Pochan, D. J. *Biochemistry* **2008**, *47*, 4597.
- (48) Borchelt, D. R.; Thinakaran, G.; Eckman, C. B.; Lee, M. K.; Davenport, F.; Ratovitsky, T.; Prada, C. M.; Kim, G.; Seekins, S.; Yager, D.; Slunt, H. H.; Wang, R.; Seeger, M.; Levey, A. I.; Gandy, S. E.; Copeland, N. G.; Jenkins, N. A.; Price, D. L.; Younkin, S. G.; Sisodia, S. S. *Neuron* **1996**, *17*, 1005.
- (49) Garcia-Alloza, M.; Robbins, E. M.; Zhang-Nunes, S. X.; Purcell, S. M.; Betensky, R. A.; Raju, S.; Prada, C.; Greenberg, S. M.; Bacskai, B. J.; Frosch, M. P. *Neurobiol. Dis.* **2006**, *24*, 516.
- (50) Delatour, B.; Guegan, M.; Volk, A.; Dhenain, M. *Neurobiol. Aging* **2006**, *27*, 835.
- (51) Smith, D. P.; Smith, D. G.; Curtain, C. C.; Boas, J. F.; Pilbrow, J. R.; Ciccotosto, G. D.; Lau, T. L.; Tew, D. J.; Perez, K.; Wade, J. D.; Bush, A. I.; Drew, S. C.; Separovic, F.; Masters, C. L.; Cappai, R.; Barnham, K. J. *J. Biol. Chem.* **2006**, *281*, 15145.
- (52) Klug, G. M.; Losic, D.; Subasinghe, S. S.; Aguilar, M. I.; Martin, L. L.; Small, D. H. *Eur. J. Biochem.* **2003**, *270*, 4282.
- (53) Opazo, C.; Huang, X.; Cherny, R. A.; Moir, R. D.; Roher, A. E.; White, A. R.; Cappai, R.; Masters, C. L.; Tanzi, R. E.; Inestrosa, N. C.; Bush, A. I. *J. Biol. Chem.* **2002**, *277*, 40302.
- (54) Boye-Harnasch, M.; Cullin, C. *J. Biotechnol.* **2006**, *125*, 222.
- (55) Fawver, J. N.; Duong, K. T.; Wise-Scira, O.; Petrofes Chapa, R.; Schall, H. E.; Coskuner, O.; Zhu, X.; Colom, L. V.; Murray, I. V. *J. Alzheimer's Dis.* **2012**, *32*, 197.
- (56) Mathis, C. A.; Mason, N. S.; Lopresti, B. J.; Klunk, W. E. *Semin. Nucl. Med.* **2012**, *42*, 423.
- (57) Zhang, L.; Chang, R. C.; Chu, L. W.; Mak, H. K. *Am. J. Nucl. Med. Mol. Imaging* **2012**, *2*, 386.
- (58) Kuntner, C.; Kesner, A. L.; Bauer, M.; Kremslehner, R.; Wanek, T.; Mandler, M.; Karch, R.; Stanek, J.; Wolf, T.; Muller, M.; Langer, O. *Mol. Imaging Biol.* **2009**, *11*, 236.
- (59) Maeda, J.; Ji, B.; Irie, T.; Tomiyama, T.; Maruyama, M.; Okauchi, T.; Staufenbiel, M.; Iwata, N.; Ono, M.; Saido, T. C.; Suzuki, K.; Mori, H.; Higuchi, M.; Suhara, T. *J. Neurosci.* **2007**, *27*, 10957.
- (60) Poinsel, G.; Dhilly, M.; Moustie, O.; Delamare, J.; Abbas, A.; Guilloteau, D.; Barre, L. *Neurobiol. Aging* **2012**, *33*, 2561.
- (61) Manook, A.; Yousefi, B. H.; Willuweit, A.; Platzer, S.; Reder, S.; Voss, A.; Huisman, M.; Settles, M.; Neff, F.; Velden, J.; Schoor, M.; von der Kammer, H.; Wester, H. J.; Schwaiger, M.; Henriksen, G.; Drzezga, A. *PLoS One* **2012**, *7*, e31310.
- (62) Jack, C. R., Jr.; Garwood, M.; Wengenack, T. M.; Borowski, B.; Curran, G. L.; Lin, J.; Adriany, G.; Grohn, O. H.; Grimm, R.; Poduslo, J. F. *Magn. Reson. Med.* **2004**, *52*, 1263.
- (63) Klunk, W. E.; Engler, H.; Nordberg, A.; Wang, Y.; Blomqvist, G.; Holt, D. P.; Bergstrom, M.; Savitcheva, I.; Huang, G. F.; Estrada, S.; Ausen, B.; Debnath, M. L.; Barletta, J.; Price, J. C.; Sandell, J.; Lopresti, B. J.; Wall, A.; Koivisto, P.; Antoni, G.; Mathis, C. A.; Langstrom, B. *Ann. Neurol.* **2004**, *55*, 306.
- (64) Higuchi, M.; Iwata, N.; Matsuba, Y.; Sato, K.; Sasamoto, K.; Saido, T. C. *Nat. Neurosci.* **2005**, *8*, 527.
- (65) Nordberg, A.; Rinne, J. O.; Kadir, A.; Langstrom, B. *Nat. Rev. Neurol.* **2010**, *6*, 78.
- (66) Hsiao, K.; Chapman, P.; Nilsen, S.; Eckman, C.; Harigaya, Y.; Younkin, S.; Yang, F.; Cole, G. *Science* **1996**, *274*, 99.
- (67) Cao, D.; Lu, H.; Lewis, T. L.; Li, L. *J. Biol. Chem.* **2007**, *282*, 36275.
- (68) Masuda, Y.; Fukuchi, M.; Yatagawa, T.; Tada, M.; Takeda, K.; Irie, K.; Akagi, K.; Monobe, Y.; Imazawa, T.; Takegoshi, K. *Bioorg. Med. Chem.* **2011**, *19*, 5967.
- (69) Wadhvani, P.; Strandberg, E.; Heidenreich, N.; Burck, J.; Fanghanel, S.; Ulrich, A. S. *J. Am. Chem. Soc.* **2012**, *134*, 6512.
- (70) Paravastu, A. K.; Leapman, R. D.; Yau, W. M.; Tycko, R. *Proc. Natl. Acad. Sci. U.S.A.* **2008**, *105*, 18349.
- (71) Ahmed, M.; Davis, J.; Aucoin, D.; Sato, T.; Ahuja, S.; Aimoto, S.; Elliott, J. I.; Van Nostrand, W. E.; Smith, S. O. *Nat. Struct. Mol. Biol.* **2010**, *17*, 561.
- (72) Urbanc, B.; Betnel, M.; Cruz, L.; Bitan, G.; Teplow, D. B. *J. Am. Chem. Soc.* **2010**, *132*, 4266.
- (73) Bertini, I.; Gonnelli, L.; Luchinat, C.; Mao, J.; Nesi, A. *J. Am. Chem. Soc.* **2011**, *133*, 16013.
- (74) Liu, G.; Prabhakar, A.; Aucoin, D.; Simon, M.; Sparks, S.; Robbins, K. J.; Sheen, A.; Petty, S. A.; Lazo, N. D. *J. Am. Chem. Soc.* **2010**, *132*, 18223.
- (75) Fawzi, N. L.; Ying, J.; Torchia, D. A.; Clore, G. M. *J. Am. Chem. Soc.* **2010**, *132*, 9948.
- (76) Antzutkin, O. N.; Iuga, D.; Filippov, A. V.; Kelly, R. T.; Becker-Baldus, J.; Brown, S. P.; Dupree, R. *Angew. Chem.* **2012**, *51*, 10289.

- (77) Scheidt, H. A.; Morgado, I.; Rothmund, S.; Huster, D.; Fandrich, M. *Angew. Chem.* **2011**, *50*, 2837.
- (78) Sinha, S.; Lopes, D. H.; Du, Z.; Pang, E. S.; Shanmugam, A.; Lomakin, A.; Talbiersky, P.; Tennstaedt, A.; McDaniel, K.; Bakshi, R.; Kuo, P. Y.; Ehrmann, M.; Benedek, G. B.; Loo, J. A.; Klarner, F. G.; Schrader, T.; Wang, C.; Bitan, G. *J. Am. Chem. Soc.* **2011**, *133*, 16958.
- (79) Zhuang, T.; Jap, B. K.; Sanders, C. R. *J. Am. Chem. Soc.* **2011**, *133*, 20571.
- (80) Fawzi, N. L.; Ying, J.; Ghirlando, R.; Torchia, D. A.; Clore, G. M. *Nature* **2011**, *480*, 268.
- (81) Strodel, B.; Lee, J. W.; Whittleston, C. S.; Wales, D. J. *J. Am. Chem. Soc.* **2010**, *132*, 13300.
- (82) Rangachari, V.; Moore, B. D.; Reed, D. K.; Sonoda, L. K.; Bridges, A. W.; Conboy, E.; Hartigan, D.; Rosenberry, T. L. *Biochemistry* **2007**, *46*, 12451.
- (83) Moore, B. D.; Rangachari, V.; Tay, W. M.; Milkovic, N. M.; Rosenberry, T. L. *Biochemistry* **2009**, *48*, 11796.
- (84) Yiannopoulou, K. G.; Papageorgiou, S. G. *Ther. Adv. Neurol. Disord.* **2013**, *6*, 19.
- (85) McLaurin, J.; Kierstead, M. E.; Brown, M. E.; Hawkes, C. A.; Lambermon, M. H.; Phinney, A. L.; Darabie, A. A.; Cousins, J. E.; French, J. E.; Lan, M. F.; Chen, F.; Wong, S. S.; Mount, H. T.; Fraser, P. E.; Westaway, D.; St. George-Hyslop, P. *Nat. Med.* **2006**, *12*, 801.
- (86) Stefani, M.; Dobson, C. M. *J. Mol. Med. (Berlin)* **2003**, *81*, 678.
- (87) Yang, W.; Wong, Y.; Ng, O. T.; Bai, L. P.; Kwong, D. W.; Ke, Y.; Jiang, Z. H.; Li, H. W.; Yung, K. K.; Wong, M. S. *Angew. Chem.* **2012**, *51*, 1804.
- (88) Frydman-Marom, A.; Rechter, M.; Shefler, I.; Bram, Y.; Shalev, D. E.; Gazit, E. *Angew. Chem.* **2009**, *48*, 1981.
- (89) Cheng, P. N.; Spencer, R.; Woods, R. J.; Glabe, C. G.; Nowick, J. S. *J. Am. Chem. Soc.* **2012**, *134*, 14179.
- (90) Yang, F.; Lim, G. P.; Begum, A. N.; Ubeda, O. J.; Simmons, M. R.; Ambegaokar, S. S.; Chen, P. P.; Kaye, R.; Glabe, C. G.; Frautschy, S. A.; Cole, G. M. *J. Biol. Chem.* **2005**, *280*, 5892.
- (91) Sievers, S. A.; Karanicolas, J.; Chang, H. W.; Zhao, A.; Jiang, L.; Zirafi, O.; Stevens, J. T.; Munch, J.; Baker, D.; Eisenberg, D. *Nature* **2011**, *475*, 96.
- (92) Bieschke, J.; Herbst, M.; Wiglenda, T.; Friedrich, R. P.; Boeddrich, A.; Schiele, F.; Kleckers, D.; Lopez del Amo, J. M.; Gruning, B. A.; Wang, Q.; Schmidt, M. R.; Lurz, R.; Anwyll, R.; Schnoegl, S.; Fandrich, M.; Frank, R. F.; Reif, B.; Gunther, S.; Walsh, D. M.; Wanker, E. E. *Nat. Chem. Biol.* **2012**, *8*, 93.
- (93) Nacula, M.; Kaye, R.; Milton, S.; Glabe, C. G. *J. Biol. Chem.* **2007**, *282*, 10311.
- (94) Ladiwala, A. R.; Dordick, J. S.; Tessier, P. M. *J. Biol. Chem.* **2011**, *286*, 3209.
- (95) Trippier, P. C.; Jansen Labby, K.; Hawker, D. D.; Mataka, J. J.; Silverman, R. B. *J. Med. Chem.* **2013**, *56*, 3121.
- (96) Zhou, Y.; Jiang, C.; Zhang, Y.; Liang, Z.; Liu, W.; Wang, L.; Luo, C.; Zhong, T.; Sun, Y.; Zhao, L.; Xie, X.; Jiang, H.; Zhou, N.; Liu, D.; Liu, H. *J. Med. Chem.* **2010**, *53*, 5449.
- (97) Orlando, R. A.; Gonzales, A. M.; Royer, R. E.; Deck, L. M.; Vander Jagt, D. L. *PLoS One* **2012**, *7*, e31869.
- (98) Landau, M.; Sawaya, M. R.; Faull, K. F.; Laganowsky, A.; Jiang, L.; Sievers, S. A.; Liu, J.; Barrio, J. R.; Eisenberg, D. *PLoS Biol.* **2011**, *9*, e1001080.
- (99) Hobart, L. J.; Seibel, I.; Yeargans, G. S.; Seidler, N. W. *Life Sci.* **2004**, *75*, 1379.
- (100) LeVine, H., 3rd; Ding, Q.; Walker, J. A.; Voss, R. S.; Augelli-Szafran, C. E. *Neurosci. Letters.* **2009**, *465*, 99.
- (101) Klunk, W. E.; Lopresti, B. J.; Ikonovic, M. D.; Lefterov, I. M.; Koldamova, R. P.; Abrahamson, E. E.; Debnath, M. L.; Holt, D. P.; Huang, G. F.; Shao, L.; DeKosky, S. T.; Price, J. C.; Mathis, C. A. *J. Neurosci.* **2005**, *25*, 10598.
- (102) Gregory, G. C.; Halliday, G. M. *Neurotoxic. Res.* **2005**, *7*, 29.
- (103) Stine, W. B., Jr.; Dahlgren, K. N.; Krafft, G. A.; LaDu, M. J. *J. Biol. Chem.* **2003**, *278*, 11612.
- (104) Zhang, C.; Browne, A.; Child, D.; Divito, J. R.; Stevenson, J. A.; Tanzi, R. E. *J. Biol. Chem.* **2010**, *285*, 8515.
- (105) Hiltunen, M.; Lu, A.; Thomas, A. V.; Romano, D. M.; Kim, M.; Jones, P. B.; Xie, Z.; Kounnas, M. Z.; Wagner, S. L.; Berezovska, O.; Hyman, B. T.; Tesco, G.; Bertram, L.; Tanzi, R. E. *J. Biol. Chem.* **2006**, *281*, 32240.